12-2022

Lifting-Line Predictions for Life and Twist Distributions to Minimize Induced Drag in Ground Effect

Kyler Church
Utah State University

LIFTING-LINE PREDICTIONS FOR LIFT AND TWIST DISTRIBUTIONS TO MINIMIZE INDUCED DRAG IN GROUND EFFECT

by

Kyler Church

A thesis submitted in partial fulfillment
of the requirements for the degree

of

MASTER OF SCIENCE

in

Aerospace Engineering

Approved:

Douglas F. Hunsaker, Ph.D. Major Professor	Stephen A. Whitmore, Ph.D. Committee Member
Tianye He, Ph.D. Committee Member	D. Richard Cutler, Ph.D. Vice Provost of Graduate Studies

UTAH STATE UNIVERSITY
Logan, Utah

2022

ABSTRACT

Lifting-Line Predictions for Lift and Twist Distributions to Minimize Induced Drag in Ground Effect

by

Kyler Church, Master of Science

Utah State University, 2022

Major Professor: Douglas F. Hunsaker, Ph.D.
Department: Mechanical and Aerospace Engineering

The elliptic lift distribution produces the minimum induced drag for a given wingspan and desired lift outside of ground effect. This distribution can be generated on any wing by using geometric and/or aerodynamic twist. However, in ground effect, the elliptic lift distribution is not necessarily that which minimizes induced drag. The present work uses a modern numerical lifting-line algorithm to evaluate how the optimum lift distribution varies as a function of height above ground for a rectangular wing. The results of this work can be used to reduce takeoff distances on morphing wings or wings that can actively change twist or camber during flight. It was found that in ground effect, the lift is shifted inboard while the induced drag is shifted outboard. Optimally twisting the wing in ground effect significantly reduces the induced drag compared to the untwisted wing. However, the twist distribution found to achieve this minimum induced drag was nearly identical to the twist distribution needed to achieve an elliptic lift distribution out of ground effect for a rectangular wing, except when the wing is extremely close to the ground.

(76 pages)

PUBLIC ABSTRACT

Lifting-Line Predictions for Lift and Twist Distributions to Minimize Induced Drag in Ground Effect

Kyler Church

The elliptic lift distribution produces the minimum induced drag for a given wingspan and desired lift outside of ground effect. This distribution can be generated on any wing by using geometric and/or aerodynamic twist. However, in ground effect, the elliptic lift distribution is not necessarily that which minimizes induced drag. The present work uses a modern numerical lifting-line algorithm to evaluate how the optimum lift distribution varies as a function of height above ground. The algorithm is also used to obtain the twist distributions that should be applied to wings of varying aspect ratios and taper ratios to produce the optimum lift distribution in ground effect. The results of this work can be used to reduce takeoff distances on morphing wings, or wings that can actively change twist or camber during flight.

CONTENTS

LIST OF TABLES

LIST OF FIGURES

ACRONYMS

IGE	in ground effect
OGE	out of ground effect
SLSQP	sequential least squares programming

NOMENCLATURE

A_j	=	Fourier coefficients in the lifting-line solution for section-lift, Eq. (1.1)
a_j	=	decomposed Fourier-series coefficients related to planform, Eq. (1.11)
B_j	=	normalized Fourier coefficients in lifting-line solution for section-lift
b	=	wingspan
b_j	=	decomposed Fourier-series coefficients related to twist, Eq. (1.13)
c	=	local wing section chord length
$\overline{c}$	=	mean geometric chord
$\tilde{C}_{L,\alpha}$	=	wing section-lift slope
C_{Di}	=	wing induced drag coefficient
$\tilde{C}_{Di}$	=	section induced drag coefficient
$\hat{C}_{Di}$	=	normalized section induced drag coefficient
C_L	=	wing lift coefficient
$\tilde{C}_L$	=	section lift coefficient
$\hat{C}_L$	=	normalized section lift coefficient
c_{ref}	=	reference chord length
c_{root}	=	chord length at root of wing
c_{tip}	=	chord length at tip of wing
D_i	=	wing induced drag
$\tilde{F}_{\hat{x}}$	=	aerodynamic force in the direction of $\hat{x}$
$\tilde{F}_{\hat{z}}$	=	aerodynamic force in the direction of $\hat{z}$
h	=	height of the wing above the ground
$\tilde{L}$	=	section lift
N	=	number of twist locations per semispan
R_A	=	wing aspect ratio
R_T	=	wing taper ratio
V_i	=	total velocity vector induced at control point i, Eq. (3.1)
V_∞	=	freestream airspeed
v_{ji}	=	velocity vector induced at control point i by vortex j
W	=	weight of aircraft
$\hat{x}$	=	coordinate system component defined in axial direction in MachUpX
z	=	spanwise coordinate relative to the mid-span
$\hat{z}$	=	coordinate system component defined in normal direction in MachUpX
α	=	aerodynamic angle of attack
α_{eff}	=	local section angle of attack
α_{L0}	=	zero-lift angle of attack
α_{root}	=	angle of attack at wing root
β	=	empirical correction coefficient, Eq. (1.45)
β_L, β_D	=	tapered-wing correction coefficients, Eqs. (1.48) and (1.49)
Γ_j	=	strength of horseshoe vortex j, Eq. (3.1)

δ_L, δ_D	=	tapered-wing correction coefficients, Eqs. (1.50) and (1.51)
θ	=	change of variables along the spanwise coordinate, Eq. (1.2)
κ_D	=	planform contribution to the induced drag factor, Eq. (1.23)
ρ	=	air density
Ω	=	amount of the symmetric component of wing twist, Eq. (1.30)
ω	=	spanwise distribution function for component of wing twist, Eq. (1.29)

CHAPTER 1
INTRODUCTION

The elliptic lift distribution produces the minimum induced drag for a given wingspan and lift outside of ground effect [1–3]. This lift distribution can be produced by any wing by applying wing twist [4–7]. However, most aircraft spend some time in ground effect due to the need to take off and land on the ground, and some aircraft are even designed to fly exclusively in ground effect [8, 9].

When a wing is near the ground, the induced angle of attack due to the shed vorticity in the wing wake is reduced [8,10,11]. This alters the lift distribution [8], and likely changes the optimum lift distribution that would minimize induced drag. Because the optimum lift distribution in ground effect can vary significantly from the elliptic lift distribution, it may be beneficial for some aircraft to operate at a different lift distribution during takeoff in order to minimize thrust required, fuel burn, and ground roll.

Several research agencies have recently studied aircraft that have the ability to actively change wing twist during flight [12–15]. Such aircraft could potentially use an optimal twist distribution during takeoff and landing, and employ a different optimum twist distribution and lift distribution during other flight phases. The purpose of the present work is to identify optimum lift distributions in ground effect that minimize induced drag and to evaluate the appropriate twist distributions that can be applied to rectangular wings to produce these optimum distributions. To better understand these optimum distributions, it is helpful to review the theoretical relationship between lift distribution and induced drag.

1.1 Theory of lift and induced drag

Prandtl's classical lifting line theory [1, 2] shows that an arbitrary spanwise section-lift distribution for a finite wing with no sweep or dihedral can be written as a Fourier sine

series. Combining the Kutta-Joukowski law [16, 17] with the classical lifting-line solution for the spanwise section-circulation distribution gives

$$\tilde{L}(\theta) = 2\rho V_\infty^2 b \sum_{j=1}^{\infty} A_j \sin(j\theta) \tag{1.1}$$

where θ is a change of variables along the spanwise coordinate z

$$\theta \equiv \cos^{-1}\left(-\frac{2z}{b}\right) \tag{1.2}$$

The sign convention for the spanwise coordinate z is positive out the left wing. Prandtl's classical lifting-line equation relates the section-lift distribution to the spanwise chord-length and aerodynamic-angle-of-attack distribution for a finite wing with no dihedral or sweep immersed in a uniform flow. For a given wing planform with a given twist distribution, the lifting-line equation can be used to obtain the spanwise section-lift distribution [4,5,18–22].

The Fourier coefficients A_j in Eq.(1.1) are obtained by forcing the lifting-line equation to be satisfied at a finite number of (N) locations along the wing. The result of forcing the lifting-line equation to be satisfied for a finite number of elements is a linear system of equations that can be solved for the truncated Fourier series

$$\sum_{j=1}^{\infty} A_j \left[\frac{4b}{\tilde{C}_{L,\alpha} c(\theta)} + \frac{j}{\sin(\theta)}\right] \sin(j\theta) = \alpha(\theta) - \alpha_{L0}(\theta) \tag{1.3}$$

The right-hand side of Eq.(1.3) represents the aerodynamic-angle-of-attack distribution, which is the local spanwise section angle of attack minus the section zero-lift angle of attack. This distribution can be manipulated by aerodynamic wing twist, such as a change in airfoil section as a function of spanwise location, geometric twist, and/or control-surface deflection. From the definitions of lift coefficient, drag coefficient, and aspect ratio, the lifting-line solution gives

$$C_L = \pi R_A A_1 \tag{1.4}$$

$$C_{Di} = \pi R_A \sum_{j=1}^{\infty} j A_j^2 = \frac{C_L^2}{\pi R_A} + \pi R_A \sum_{j=2}^{\infty} j A_j^2 \tag{1.5}$$

Note that A_1 used in Eq.(1.4) only contributes to the net lift whereas all of the Fourier Coefficients A_j contribute to the induced drag. However, the lifting-line solution presented in Eq.(1.4) and (1.5) is cumbersome for evaluating traditional wing properties because the Fourier coefficients depend on angle of attack and must be reevaluated at each operating point studied. For a wing with no twist [23], α and α_{L0} are independent of θ and the Fourier coefficients shown in Eq.(1.5) which can be written as

$$A_j \equiv a_j(\alpha - \alpha_{L0}) \tag{1.6}$$

However, for wings with aerodynamic or geometric twist, the aerodynamic angle of attack, $\alpha - \alpha_0$ is not constant along the span and the relation given by Eq.(1.6) cannot be applied. The procedure commonly used for lifting-line analysis of wings with twist is based on the Eqs.(1.1-1.5) and requires evaluating separate sets of Fourier Coefficients A_j at different angles of attack.

A more practical form of the lifting-line solution for twisted wings was presented by Phillips [22] and can be obtained by using the change of variables

$$\alpha(\theta) - \alpha_{L0}(\theta) \equiv (\alpha - \alpha_{L0})_{\text{root}} - \Omega\omega(\theta) \tag{1.7}$$

where Ω is defined to be the maximum total washout, geometric plus aerodynamic

$$\Omega \equiv (\alpha - \alpha_{L0})_{\text{root}} - (\alpha - \alpha_{L0})_{\max} \tag{1.8}$$

and $\omega(\theta)$ is the washout distribution normalized with respect to the maximum total washout

$$\omega(\theta) \equiv \frac{\alpha(\theta) - \alpha_{L0}(\theta) - (\alpha - \alpha_{L0})_{\text{root}}}{(\alpha - \alpha_{L0})_{\max} - (\alpha - \alpha_{L0})_{\text{root}}} \tag{1.9}$$

This results in the normalized washout distribution function $\omega(\theta)$ being independent of

angle of attack and varies from 0.0 at the root to 1.0 at the point of maximum washout, which is commonly at the wingtips [22]. Using Eq.(1.7) in Eq.(1.8) gives

$$\sum_{j=1}^{\infty} A_j \left[1 + \frac{\tilde{C}_{L,\alpha} c(\theta)}{4b \sin(\theta)} \right] \sin(j\theta) = \frac{\tilde{C}_{L,\alpha} c(\theta)}{4b} \left[(\alpha - \alpha_{L0})_{\text{root}} - \Omega\omega(\theta) \right] \tag{1.10}$$

the Fourier coefficients A_j in Eq.(1.10) can be expressed by

$$A_j \equiv a_j (\alpha - \alpha_{L0})_{\text{root}} - b_j \Omega \tag{1.11}$$

where the decomposed Fourier coefficients a_j and b_j can be computed from the relations

$$\sum_{j=1}^{\infty} a_j \left[\frac{4b}{\tilde{C}_{L,\alpha} c(\theta)} + \frac{j}{\sin(\theta)} \right] \sin(j\theta) = 1 \tag{1.12}$$

$$\sum_{j=1}^{\infty} b_j \left[\frac{4b}{\tilde{C}_{L,\alpha} c(\theta)} + \frac{j}{\sin(\theta)} \right] \sin(j\theta) = \omega(\theta) \tag{1.13}$$

An important note to understand is that the decomposed Fourier coefficients in Eq.(1.12) and Eq.(1.13) are all independent of angle of attack and symmetric twist magnitude. Meaning that for a given wing geometry and symmetric twist distribution function, Eq.(1.12) and Eq.(1.13) can be solved for the decomposed Fourier coefficients. These coefficients, along with the angle of attack and symmetric twist magnitude can then be used in Eq. (1.11) to compute the Fourier coefficients needed in Eq.(1.4) and Eq.(1.5).

Using Eq.(1.11) in Eq.(1.1), along with the definitions of section lift coefficient and wing aspect ratio, the section lift coefficient as a function of spanwise coordinate can be computed from the linear combination

$$\tilde{C}_L(\theta) = \frac{\tilde{L}(\theta)}{\frac{1}{2}\rho V_\infty^2 \bar{c}} = 4R_A \left[(\alpha - \alpha_{L0})_{\text{root}} \sum_{j=1}^{\infty} a_j \sin(j\theta) - \Omega \sum_{j=1}^{\infty} b_j \sin(j\theta) \right] \tag{1.14}$$

If the wing is spanwise symmetric in geometry, the even terms of the a_j coefficients will be zero. Likewise, because $\omega(\theta)$ is a symmetric twist distribution function, the even terms of the b_j coefficients will be zero. Therefore, Eq.(1.11) reduces to

$$A_j = \begin{cases} a_j(\alpha - \alpha_{L0})_{\text{root}} - b_j\omega(\theta), & j \quad \text{odd} \\ 0 & j \quad \text{even} \end{cases} \tag{1.15}$$

Using Eq.(1.11) in Eq.(1.4) within the small-angle approximation of lifting-line theory, we see that the lift coefficient C_L can be written in terms of a_j and b_j

$$C_L = \pi R_A[a_1(\alpha - \alpha_{L0})_{\text{root}} - b_1\Omega] \tag{1.16}$$

From Eq.(1.15) and Eq.(1.16), we see that only the a_j and b_j terms contribute to the lift and odd terms of A_j. Using Eq.(1.11) in Eq.(1.5) within the small-angle approximation of lifting-line theory, we see that the induced drag coefficient C_{Di} can be written in terms of a_j and b_j. We then use Eq.(1.11) in Eq.(1.5) which yields the following formulation for the induced-drag coefficient

$$C_{Di} = \pi R_A \sum_{j=1}^{\infty} j A_j^2 = \pi R_A \left[a_1(\alpha - \alpha_{L0})_{\text{root}} - b_1\Omega\right]^2 + \pi R_A \sum_{j=2}^{\infty} j \left[a_j(\alpha - \alpha_{L0})_{\text{root}} - b_j\Omega\right]^2 \tag{1.17}$$

or in view of Eq.(1.16)

$$C_{Di} = \frac{C_L^2}{\pi R_A} + \pi R_A \sum_{j=2}^{\infty} j \left[a_j^2(\alpha - \alpha_{L0})_{\text{root}}^2 - 2a_j b_j(\alpha - \alpha_{L0})_{\text{root}}\Omega + b_j^2\Omega^2\right] \tag{1.18}$$

With this lifting-line formulation, we shall now consider optimal lift distributions for minimum induced drag outside of ground effect.

1.2 Optimum Lift Distributions

According to Prandtl's traditional lifting-line theory, the elliptic lift distribution minimizes induced drag on a single straight wing with a given wingspan and desired lift [1–3].

Prandtl showed this in 1921 in a report translated into English by the National Advisory Committee for Aeronautics [2]. Prandtl expressly stated in this report that the elliptic lift distribution is optimum only "for a monoplane with given values for total lift, the span, and the velocity."

For an elliptic planform, the lift distribution as a function of spanwise coordinate is given by

$$\tilde{C}_L(\theta) = \frac{4}{\pi} C_L \sin(\theta) \tag{1.19}$$

and the chord length varies with spanwise coordinate and can be calculated using

$$c(z) = \left[\frac{4b}{(\pi R_A)}\right] \sqrt{1 - \left(\frac{2z}{b}\right)^2} \tag{1.20}$$

or using the change of variables from Eq.(1.2)

$$c(\theta) = \left[\frac{4b}{(\pi R_A)}\right] \sin(\theta) \tag{1.21}$$

As stated previously, the planform shape that produces the least amount of induced drag for a given lift coefficient and aspect ratio is an elliptic wing with no geometric or aerodynamic twist. [5] This can be shown by writing the equation for the induced drag C_{Di} as [4]

$$C_{Di} = \pi R_A \sum_{j=1}^{\infty} j A_j^2 = \frac{C_L^2}{\pi R_A}(1 + \kappa_D) \tag{1.22}$$

where κ_D is the planform contribution to the induced-drag factor and is equal to

$$\kappa_D = \sum_{j=2}^{\infty} j \left(\frac{A_j}{A_1}\right)^2 \tag{1.23}$$

For an elliptic wing with zero twist, κ_D is equal to zero, which yields the following equation for induced drag

$$C_{Di} = \frac{C_L^2}{\pi R_A} \tag{1.24}$$

As stated previously, the minimum possible value for the planform contribution factor κ_D is zero, which occurs when having $A_j = 0$ for all $j \geq 2$. If $A_j \neq 0$ for $j \geq 2$, κ_D will be greater than zero which increases the induced drag coefficient C_{Di}. For this reason, the elliptic lift distribution is the distribution of lift that minimizes the induced drag.

However, as Prandtl [3] points out, imposing the constraints of fixed gross weight and wingspan when designing a wing to minimize induced drag in steady level flight does not result in an absolute minimum in induced drag. Other optimal distributions exist which include the effects of structural constraints on the wing [24].

The lift distribution and induced drag given earlier in Eq.(1.19) and Eq.(1.22) can be written in many different forms. However, for the purpose of accounting for weight in their analysis, Phillips [24] used

$$\frac{b\tilde{L}(\theta)}{L} = \frac{4}{\pi}\left[\sin(\theta) + \sum_{j=2}^{N} B_j \sin(j\theta)\right] \tag{1.25}$$

and

$$D_i = \frac{2\left(\frac{W}{b}\right)^2}{\pi\rho V_\infty^2}\left(1 + \sum_{j=2}^{\infty} jB_j^2\right) \tag{1.26}$$

where the B_j term seen in Eq.(1.25) are Fourier coefficients and are simply defined as $B_j = A_j/A_1$.

Prandtl was the first to consider the variational problem of designing a wing that produces an absolute minimum in induced drag [3]. Prandtl found an analytic solution for the fixed lift distribution that minimizes induced drag under the constraints of fixed gross lift and fixed moment of inertia of gross lift, but no constraint on the wingspan. Prandtl's 1933 solution for minimizing induced drag under these constraints yields the dimensionless section-lift distribution [3]

$$\frac{b\tilde{L}(\theta)}{L} = \frac{4}{\pi}\left[\sin(\theta) - \frac{1}{3}\sin(3\theta)\right] \tag{1.27}$$

By comparing Eq.(1.25) and Eq.(1.27), we see that Eq.(1.27) requires that $B_3 = -1/3$ and $B_j = 0$ for all $j \neq 3$. Using the Fourier coefficients in Eq.(1.26) yields the induced drag in steady level flight for Prandtl's 1933 [3] lift distribution

$$D_i = \frac{8\left(\frac{W}{b}\right)^2}{3\pi\rho V_\infty^2} \tag{1.28}$$

By comparing Eq.(1.26) and Eq.(1.28), we see that Prandtl's 1933 lift distribution produces more induced drag than the elliptic lift distribution if the weight and wingspan are fixed. However, it is important to note that Prandtl did not claim that the lift distribution in Eq.(1.27) yields an absolute minimum in induced drag for any particular case of a physical wing. [1, 3]. He only claimed that this lift distribution minimizes induced drag under the constraints of fixed gross lift and fixed moment of inertia. Some other values for the term B_3 yield different lift distributions. For example, $B_3 = 0$ yields the elliptic lift distribution while $B_3 = 1/3$ yields a bell curve lift distribution [1, 3].

While there are other optimal lift distributions when accounting for structural constraints such as wingspan and weight, this research will focus on the elliptic lift distribution with equations that are not dependent on any structural constraints.

1.3 Twist For Optimum Lift Distributions

A closed-form analytic solution published by Phillips [6] shows that there is a symmetric baseline twist distribution, amount, and angle of attack for any given wing planform that minimizes the induced drag at a prescribed lift coefficient and zero roll and yaw [4–7].

The twist distribution can be manipulated using several different methods, such as a change in airfoil section as a function of spanwise location, geometric twist, and/or control-surface deflection. All of these methods can affect the twist distribution, but each method produces the identical aerodynamic effect with respect to the approximations of the classical lifting-line theory. Because of this, any method used to manipulate the twist distribution will be referred to as "washout" for the remainder of this research with the understanding that it could be any of the previously mentioned methods.

The symmetric wing washout distribution function for any given wing planform that minimizes induced drag in steady level flight is [4, 5, 22]

$$\omega(\theta) = 1 - \frac{\sin(\theta)}{\left(\frac{c(\theta)}{c_{\text{root}}}\right)} \tag{1.29}$$

and the amount of symmetric washout required is dependent on the lift coefficient [4]

$$\Omega = \frac{4bC_L}{\pi R_A \tilde{C}_{L,\alpha} c_{\text{root}}} \tag{1.30}$$

The associated angle of attack at the root is

$$(\alpha - \alpha_{L0})_{\text{root}} = \frac{C_L}{\pi R_A}\left[\frac{4b}{\tilde{C}_{L,\alpha} c_{\text{root}}} + 1\right] \tag{1.31}$$

In steady level flight, any wing planform using the symmetric twist distribution function of Eq. (1.19) and the symmetric twist magnitude of Eq. (1.20) at the angle of attack of from Eq. (1.21) will produce an elliptic lift distribution, i.e.

$$\tilde{C}_L(\theta) = \frac{4}{\pi} C_L \sin(\theta) \tag{1.32}$$

As stated previously [1–3], this lift distribution minimizes the induced drag during steady level flight, which is of interest when designing wings for minimum induced drag [25]. For this particular case where $B_j = 0$ for all $j \neq 3$, Phillips [7] developed equations that can be used to obtain the twist distribution required to produce an arbitrary section-lift distribution across the span of an unswept wing of arbitrary planform. These equations are given by

$$\omega(\theta) = \frac{\left(\frac{4b}{\tilde{C}_{L,\alpha}}\right)\left[\left(\frac{1-B_3}{c_{\text{root}}}\right) - \left(\frac{\sin(\theta)+B_3\sin(3\theta)}{c(\theta)}\right)\right] - 3B_3\left[1 + \left(\frac{\sin(3\theta)}{\sin(\theta)}\right)\right]}{\left[\frac{4b(1-B_3)}{\tilde{C}_{L,\alpha} c_{\text{root}}}\right] - 12B_3} \tag{1.33}$$

$$\Omega = \frac{C_L}{\pi R_A}\left[\frac{4b\,(1-B_3)}{\tilde{C}_{L,\alpha} c_{\text{root}}} - 12B_3\right] \tag{1.34}$$

$$(\alpha - \alpha_{L0})_{\text{root}} = \frac{C_L}{\pi R_A}\left[\frac{4b\,(1 - B_3)}{\tilde{C}_{L,\alpha} c_{\text{root}}} + 1 - 3B_3\right] \tag{1.35}$$

1.4 Ground Effect

When the aircraft's lifting surface is in close proximity to the ground, the aerodynamic characteristics are known to be affected which is referred to as "ground effect". In ground effect, the aircraft's lifting surface will typically see an increase in lift and a decrease in induced drag [8]. One estimate that can be used for the influence of ground effect on lift is the ratio of the lift in ground effect to that of the lift out of ground effect both computed at the same angle of attack. This influence ratio is given by

$$lift\ ground\text{-}effect\ influence\ ratio \equiv \frac{[C_L(\alpha)]_h}{[C_L(\alpha)]_\infty} \tag{1.36}$$

where h is the height of the wing above the ground.

The induced drag coefficient C_{Di} is proportional to the lift coefficient squared for wings of arbitrary planform with no geometric or aerodynamic twist. Because of this relationship between the lift and drag coefficients, one common method of quantifying the effect of ground effect on induced drag is by comparing ratios of the induced-drag coefficient divided by the lift coefficient squared evaluated in ground effect to that same ratio out of ground effect. This ratio is known as the induced–drag ground-effect influence ratio and is given by

$$induced\text{-}drag\ ground\text{-}effect\ influence\ ratio \equiv \frac{\left(\frac{C_{Di}}{C_L^2}\right)_h}{\left(\frac{C_{Di}}{C_L^2}\right)_\infty} \tag{1.37}$$

Over the last 50 years, several different closed-form relations for the induced-drag ground-effect influence ratio have been recommended in aeronautics textbooks. These closed-form solutions express the ratio as a function of a single dimensionless variable h/b, where h is the height of the main wing above the ground, and b is the wingspan. One such

relation was recommended in 1975 by Hoerner and Borst [26]

$$\frac{\left(C_{Di}/C_L^2\right)_h}{\left(C_{Di}/C_L^2\right)_\infty} = \frac{33(h/b)^{1.5}}{1+33(h/b)^{1.5}} \tag{1.38}$$

In 1979, McCormick [27] presented the following relation that was slightly different than Hoerner and Borst's [26]

$$\frac{\left(C_{Di}/C_L^2\right)_h}{\left(C_{Di}/C_L^2\right)_\infty} = \frac{(16h/b)^2}{1+(16h/b)^2} \tag{1.39}$$

When comparing the results obtained from Eq.(1.38) and Eq.(1.39), Eq.(1.39) will significantly over-predict the induced-drag over the range $0.05 < h/b < 1.0$. This was attributed to a typographical error corrected in later printings of the first edition of McCormick to include π [27]

$$\frac{\left(C_{Di}/C_L^2\right)_h}{\left(C_{Di}/C_L^2\right)_\infty} = \frac{[16h/(\pi b)]^2}{1+[16h/(\pi b)]^2} \tag{1.40}$$

Errors still arose in correctly predicting the induced drag for heights above ground where $h/b < 1.0$. This led to research done in other methods to calculate the induced-drag ground-effect influence ratio. A relationship presented by Torenbeek [28] in 1982 for a case in which the wing lift coefficient is small compared to the aspect ratio is shown to become a function of the single dimensionless variable, h/b

$$\frac{\left(C_{Di}/C_L^2\right)_h}{\left(C_{Di}/C_L^2\right)_\infty} = 1 - \exp\left[-2.48(2h/b)^{0.768}\right] \tag{1.41}$$

The relation given in Eq.(1.41) agrees closely with the Hoerner and Borst [26] relation given by Eq.(1.38) over the range $h/b > 0.08$ to within about $\pm 6\%$ [8].

All of the approximations mentioned previously, such as the approximations by Hoerner and Borst [26], McCormick [29], and Torenbeek [28], are strong functions of the ratio of the wing height above ground h to the wingspan b. For this reason, Phillips and Hunsaker [8] conducted a large computational study to predict the induced drag in ground effect for

several untwisted wings of elliptic, rectangular, and tapered planforms using the numerical lifting-line method of Phillips and Snyder [30]. Results from the work done by Phillips and Hunsaker [8] showed that the Hoerner and Borst [26] and Torenbeek [28] relations are very similar to the numerical lifting-line solutions for elliptic wings. Phillips and Hunsaker [8] pointed out that the biggest discrepancy is in the $h/b > 0.07$ range, where Eq.(1.38) predicts induced drag slightly lower than Eq.(1.41) and the numerical lifting-line solutions for elliptic wings.

Using the Torenbeek [28] relation with modified coefficients, a slightly improved closed-form approximation for the mean of all numerical lifting-line solutions is obtained

$$\frac{\left(C_{Di}/C_L^2\right)_h}{\left(C_{Di}/C_L^2\right)_\infty} = 1 - \exp\left[-4.01(2h/b)^{0.717}\right] \tag{1.42}$$

By comparing Eq.(1.42) with the numerical lifting-line solutions, Phillips and Hunsaker [8] noted some scatter in the lifting-line solutions. This was due to the induced-drag ground-effect influence ratio not being a unique function of the single dimensionless variable, h/b. As a result, the induced drag predicted by Eq.(1.41) for rectangular and slightly tapered wings is somewhat low when h/b is less than about 0.4. In contrast, the values predicted for elliptic wings and wings with linear taper ratios near 0.4 are slightly high. A similar but more conservative relationship resulted by fitting only the lifting-line solutions for rectangular wings [8]

$$\frac{\left(C_{Di}/C_L^2\right)_h}{\left(C_{Di}/C_L^2\right)_\infty} = 1 - \exp\left[-3.88(2h/b)^{0.660}\right] \tag{1.43}$$

To account for the induced-drag ground-effect influence ratio not being a unique function of the single dimensionless variable h/b, Torenbeek [28] suggested a slight correction to Eq.(1.41). This correction predicts a slight increase in the influence ratio for small values of h/b in comparison to those predicted by Eq.(1.41). With this correction included, the Torenbeek [28] relation becomes a function of the wing lift coefficient, C_L, aspect ratio, R_A,

and dimensionless height, h/b

$$\frac{\left(C_{Di}/C_L^2\right)_h}{\left(C_{Di}/C_L^2\right)_\infty} = \frac{1-\exp\left[-2.48(2h/b)^{0.768}\right]}{1-\beta C_L/(4\pi R_A h/b)} \tag{1.44}$$

where

$$\beta = \sqrt{1+(2h/b)^2} - 2h/b \tag{1.45}$$

Phillips and Hunsaker [8] found that Eq.(1.44) does not give reasonable results for a region of low h/b values due to a singularity that occurs there.

When the lift coefficient is known, the closed-form approximations given by Eq.(1.42) and Eq.(1.43) provide a reasonable means of estimating the induced drag. The lift coefficient is typically known for an airplane in free flight, where the angle of attack must take the value required to support the airplane's weight at a given airspeed. However, the angle-of-attack during ground roll is typically held constant by the landing gear, and because lift is influenced by ground effect, the lift coefficient is not known a priori.

As a result, having a closed-form approximation for the induced drag and lift ground-effect influence ratio would help estimate lift and induced-drag during ground roll. In the work presented by Phillips and Hunsaker [8], closed-form relations for estimating the induced-drag and lift coefficients for untwisted wings in ground effect were developed by correlating results from numerical solutions [31] to Prandtl's lifting-line theory [1] [2] over a range of planforms, aspect ratios, and taper ratios. This produced results in good agreement with inviscid computational-fluid-dynamics solution [20] at a small fraction of the computational cost. The resulting lift and induced-drag influence ratios can be computed from

$$\frac{[C_L(\alpha)]_h}{[C_L(\alpha)]_\infty} = \frac{\left\{1+\delta_L \frac{288(h/b)^{0.787}\exp\left[-9.14(h/b)^{0.327}\right]}{R_A^{0.882}}\right\}}{\beta_L} \tag{1.46}$$

$$\frac{\left(C_{Di}/C_L^2\right)_h}{\left(C_{Di}/C_L^2\right)_\infty} = \left\{1-\delta_D \exp\left[-4.74(h/b)^{0.814}\right] - (h/b)^2 \exp\left[-3.88(h/b)^{0.758}\right]\right\}\beta_D \tag{1.47}$$

where

$$\beta_L = 1 + \frac{0.269 C_L^{1.45}}{\left[R_A^{3.18}(h/b)^{1.12}\right]} \tag{1.48}$$

$$\beta_D = 1 + \frac{0.0361 C_L^{1.21}}{\left[R_A^{1.19}(h/b)^{1.51}\right]} \tag{1.49}$$

and C_L is the lift coefficient in ground effect. The coefficients δ_D and δ_L are both 1.0 for elliptic wings. For wings with linear taper, Phillips and Hunsaker recommend

$$\delta_L = 1 - 2.25(R_T^{0.00273} - 0.997)(R_A^{0.717} + 13.6) \tag{1.50}$$

$$\delta_D = 1 - 0.157(R_T^{0.775} - 0.373)(R_A^{0.417} - 1.27) \tag{1.51}$$

Comparisons between results predicted from Eq.(1.46) and Eq.(1.47), the numerical lifting-line solutions, and results obtained from equations from Torenbeek [28], McCormick [29], and Hoerner and Borst [26] are shown in Fig. 1.1

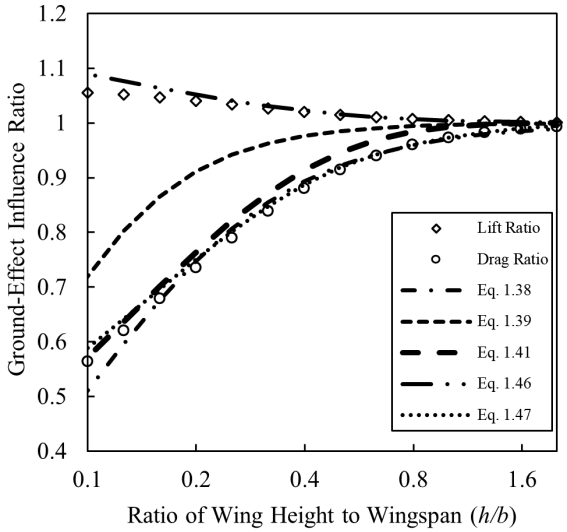

Fig. 1.1: Comparison of results obtained from Eqs. 1.38, 1.39, 1.41, 1.46, and 1.47 with results obtained from the numerical lifting-line method for a rectangular wing of aspect ratio 8 at a lift coefficient of 0.5.

As can be seen in Fig. 1.1, the closed-form relations for estimating the induced-drag and lift coefficients for untwisted wings in ground effect derived by Phillips and Hunsaker [8] are in good agreement with results obtained from the numerical lifting-line method. Also, note that as the wing gets further away from the ground, the lift and drag ratios converge to one, meaning that the wing has exited the region where the ground affects the aerodynamic characteristics of the wing.

CHAPTER 2
OBJECTIVES OF PRESENT RESEARCH

2.1 Optimal Twist Distribution in Ground Effect

Outside of the effects of ground-effect, Prandtl's traditional lifting-line theory predicts that the elliptic lift distribution minimizes induced drag on a single straight wing with a given wingspan and desired lift [1–3]. Phillip's work presents a closed-form analytic solution that shows that there is a symmetric baseline twist distribution, amount, and angle of attack for any given wing planform that minimizes the induced drag at a prescribed lift coefficient and zero roll and yaw [4–7]. Outside of ground-effect, this twist distribution produces an elliptic lift distribution.

Because the lift distribution in ground effect differs from the lift distribution out of ground effect, the closed-form solutions to optimally twist a wing to minimize induced-drag presented in Phillip's and Hunsaker's work do not apply [8]. This work seeks to find the twist distribution that produces the optimal lift distribution in ground effect that minimizes the induced drag.

The following objectives are proposed for this thesis:

1. Evaluate how the optimum lift distribution in ground effect differs from that out of ground effect

2. Obtain the twist distributions that produce the optimum lift distribution in ground effect

CHAPTER 3
APPROACH

3.1 Aerodynamic Modeling Theory

Prandtl's classical lifting-line theory, introduced in 1918, provides the basis for much of finite wing theory as we understand it today and can be used to estimate the lift distribution and induced drag on a finite wing [1]. Modeling the wing as a variable-strength bound vortex segment, known as the *lifting-line*, was central to Prandtl's theory. In the chord direction, a vortex sheet in the wing plane extended from the lifting-line to infinity. The local strength of the trailing vortex sheet was defined as the inverse of the change in strength of the bound vortex segment to satisfy Helmholtz's vortex theorems [32]. This vortex sheet induces downwash on the bound vortex segment, making the local angle of attack a function of span. Prandtl hypothesized that the lift produced due to vortex circulation at any point from a spanwise section of the wing is equivalent to that of an infinite wing of the same airfoil shape and local angle of attack as the original spanwise section.

The classical lifting line theory developed by Prandtl was the first analytical method to satisfactorily predict the performance of a finite wing. However, to obtain a tractable solution, Prandtl limited his analysis to a single wing with no sweep or dihedral [1]. This constraint allows the system of equations to be written in terms of a Fourier series, as discussed previously in this work, which can be solved for an finite number of elements N. Additionally, it caused the velocity induced by the bound vortex on the control points to be effectively zero so that it could be left out. Although Prandtl's classical lifting-line theory applies only to a single wing with no sweep or dihedral, the fundamental model upon which the theory is based can be extended to account for different variations in sweep and dihedral. For this reason, Phillips and Snyder [31] extended the work of Prandtl to include multiple

wings of arbitrary sweep and dihedral. In the development of this modern numerical lifting-line algorithm [31], Prandtl's vortex sheet is replaced with a finite number of horseshoe vortices that are placed side by side. Each horseshoe vortex consists of a straight bound segment that lies approximately along the locus of aerodynamic centers (LAC) and has two trailing segments that extend behind the wing to infinity. Each bound vortex segment also has a control point where the relevant equations are formulated and solved.

The total velocity vector induced at a control point can be determined using

$$V_i = V_{\infty_i} + \sum_{j=1}^{N} \Gamma_j v_{ji} \tag{3.1}$$

where Γ_j is the strength of horseshoe vortex j and v_{ji} is the velocity vector induced at control point i by vortex j, assuming unit vortex strength. The induced velocity is calculated using the Biot-Savart law [33]. Including the velocity induced by the bound vortex segment allows the P-S method to be used to model more complex wing geometries [33]. However, the singularities described previously are present in the method presented by Phillips and Snyder [34].

Recently, Reid and Hunsaker overcame the limitations of Phillip's and Snyder's method and presented what they termed a general numerical lifting-line method, which comprises several modifications made to the method of Phillips and Snyder which allows for wings with sweep or in sideslip [34]. Among these modifications, Reid and Hunsaker defined an effective LAC for each control point, which has zero curvature at the control point [34]. Reid and Hunsaker also added joints to the trailing vortex segments and forced these jointed portions to be perpendicular to the effective LAC [34]. With these modifications, the Reid and Hunsaker's method produces accurate results for the lift distribution on a swept wing when compared with experimental data [34, 35].

More recently, Goates and Hunsaker presented an expanded version of Reid and Hunsaker's method [36]. Goates and Hunsaker's method allows for an arbitrary number of wings with fully three-dimensional geometry. It relaxes the assumption made by Reid and Hunsaker that the chordwise circulation distribution is not a function of sweep, which predicts

no change in the section lift coefficient [34]. Goates and Hunsaker mirrored the solution scheme of the Phillips and Snyder and developed a linearized version of the general numerical lifting line equation.

3.1.1 Aerodynamic Modeling Application: MachUpX

MachUpX is a python package that implements Phillips' and Snyder's [31] numerical lifting-line algorithm with slight modifications presented by Reid and Hunsaker [34] and Goates and Hunsaker [34] to increase its accuracy and versatility. MachUpX allows for quick and accurate aerodynamic models to solve for the aerodynamic properties of fixed-wing aircraft. MachUpX is an open source code available through Github[1].

MachUpX solves the formulation of the numerical lifting-line equation presented by Reid and Hunsaker [34] which is applied to wings with sweep as shown by Goates and Hunsaker [34]. This formulation differs from the original formulation by Phillips and Snyder [31] in that the formulation is generalized to allow multiple aircraft to be analyzed at once. MachUpX sets up and solves the lifting-line equation in Earth-fixed coordinates. Once the distribution of vortex strengths is obtained, the forces and moments are integrated then transformed to the body-fixed frame for each aircraft. This algorithm produces very accurate results within the limitations of potential flow theory, without the computational overhead of higher-order methods like the vortex lattice method or CFD.

3.2 Aerodynamic Modeling Application: Case In Ground Effect

MachUpX can also be used to analyze wings in ground effect. Phillips and Hunsaker [8] provided a convenient way to analyze the effect of ground effect analytically using a model represented by Fig. 3.1.

Fig. 3.1 shows a model for simulating an aircraft in ground effect with any potential flow algorithm by replacing the ground's surface with an image of the aircraft, positioned and oriented as if it were reflected in the ground's surface. By design, the flow around this aircraft combined with its mirror image is symmetric across the plane of reflection. At any

[1] `https://github.com/usuaero/MachUpX`

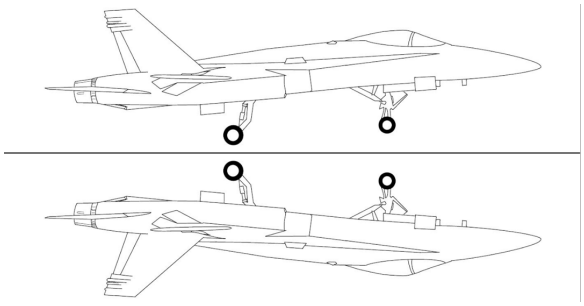

Fig. 3.1: Mirror-image model used to simulate ground effect with potential flow algorithms.

point along this plane of symmetry, the downwash generated by the aircraft will be exactly offset by the upwash generated by its mirror image.

As a result, no net flow can be normal to the plane of reflection, which is the flow's stream surface. This means that potential flow around an aircraft and its mirror image is the same as potential flow around an aircraft and a flat solid surface representing the ground. The associated aerodynamic forces will be identical because the two flows are identical. An example input file used in MachUpX to simulate ground effect is given in Appendix B.

3.3 SciPy

To minimize the induced drag, Python is used to implement the Sequential Least Squares Programming (SLSQP) minimization algorithm, a gradient-based optimization method provided by the SciPy Python library [37]. The Python interface function for the SLSQP optimization subroutine is provided in the package *scipy.optimize* and is based on the one initially implemented by Dieter Kraft [38].

One reason for selecting the SLSQP method is that in the SciPy minimization library, only the COBYLA and SLSQP local minimize methods currently support constraint arguments [37]. This allowed the optimization to be done while ensuring a lift coefficient of 0.5.

In MachUpX, wing twist is specified in a JSON file. The desired twist is specified at a specified spanwise locations (z/b). Because MachUpX linearly interpolates the intermediate values [39], the induced drag results were wavy in between twist locations. For this reason,

an alternative method was used to interpolate between twist locations. From the python package *scipy.interpolate.interp1d*, a cubic spline was selected as the method to interpolate which eliminated the waviness in the results for the values between the root and the tip. However, because this python interpolation package does not allow bounds for the end conditions, the twist and induced drag results at the root and tip may have the appearance of waves. When the total induced drag and lift were compared to the total induced drag and lift found using linearly interpolated results, they were found to be match out to five decimal places. The code was structured so that the SLSQP optimization routine changed the values of the specified twist locations within the JSON file. This was done by creating a list of twist values as the initial guess. The SLSQP optimization routine then used MachUpX to calculates and return the lift and induced drag with the modified JSON file. The twist values were then adjusted by the SLSQP optimization routine until a minimum induced drag was found for a lift coefficient of 0.5. MachUpX was solely used for calculations, and optimization was handled entirely by Python's SciPy optimization program. The code used in this work is given in Appendix E.

One important note is that the SLSQP optimization routine can find the local minimum induced drag, but does not guarantee the global minimum induced drag. This is shown in Fig. 3.2. In Fig. 3.2, the wing was initialized at three different twist distributions, one above the expected solution, one below the expected solution, and one near the expected solution using Eq. 1.29. All solutions converged to answers within 0.5% of each other. So while the SLSQP optimization routine does not guarantee the global minimum solution, the local minimum solutions are all within a range of 0.5% which is within the expected error range for lifting-line theory, which is 1.0%. The initialization input files for Fig. 3.2 can be found in Appendices A-D.

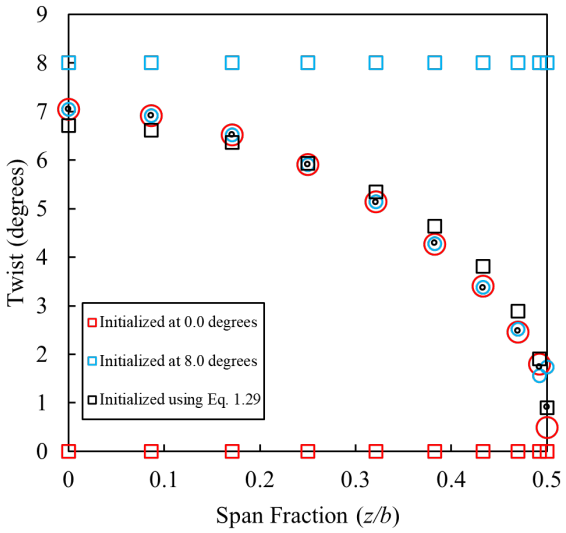

Fig. 3.2: Comparison of results for the total amount of wing twist, (Geometric wing twist + α_{root}), for an optimally twisted rectangular wing of aspect ratio 8 at a lift coefficient of 0.5 at a height above ground ratio of 0.125, ($h/b = 0.125$). Rectangular wing was initialized with zero twist, eight degrees of twist, and twisted using Eq. 1.29 represented by squares. With these initialized values, the twist was then optimized and converged to the data represented by the circles.

CHAPTER 4
GRID REFINEMENT STUDY

An analytical calculation of the induced drag was done using Eq. 1.24; this value was compared to results found using MachUpX to refine the parameters used in this work to be both accurate and time effective. The wing parameters used are given in Table 4.1. A section lift slope from thin-airfoil theory of 2π was used, and a symmetric airfoil was assumed $\alpha_{L0} = 0$.

Table 4.1: Rectangular Wing Parameters

Parameter	Value
Tolerance	$1e^{-9}$
R_A	8.0
R_T	1.0
Area [ft^2]	8.0
C_L	0.5
$\tilde{C}_{L,\alpha}$	2π
α_{L0}	0

Some parameters that needed to be refined were the number of node locations on the wing semispan, which specifies the number of horseshoe vortices used to model the wing segment in the numerical lifting-line algorithm. The default value in MachUpX is 40 [39]. The induced drag was calculated using node counts between 20-200 and compared to the analytical solution for induced drag found using Eq. 1.24. The results are shown in Fig. 4.1.

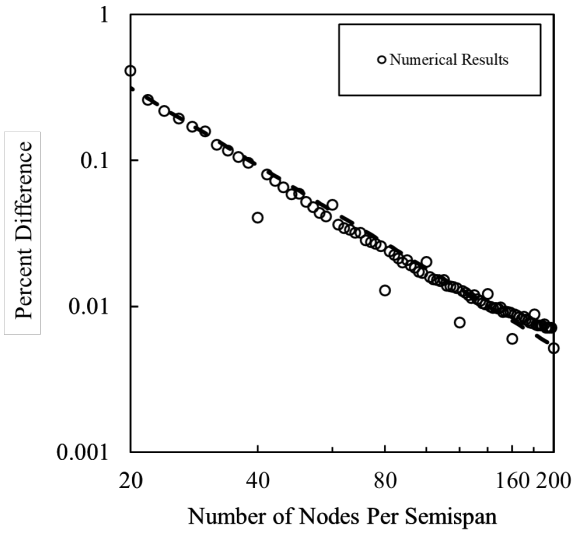

Fig. 4.1: Percent difference between the minimum induced drag found between 20-200 nodes per semispan and the analytical solution found using equation 1.24 for a rectangular wing of aspect ratio 8 at a lift coefficient of 0.5. The equation of the power line-fit to the points is $y = 62.624x^{-1.769}$.

By examining Fig. 4.1 we see that a power line-fit of the points on a log-log scale has the equation

$$y = 62.624x^{-1.769} \tag{4.1}$$

From Eq. 4.1, we note that the power is equal to -1.769, meaning that this is approaching a first order algorithm. Because lifting-line is likely only accurate to no more than 1%, the optimization in this research will use 100 nodes per semispan, providing a percent error of 0.01%. The increase in accuracy by increasing the node count to 200 nodes per semispan does not outweigh the cost in computation time.

After establishing the number of nodes per semispan that were to be used, the next step was to analyze the most accurate and time efficient number of control points to optimize the twist in the wing. Because the spanwise derivative of shed vorticity is greater in the region near the wingtips, the twist locations should be clustered more tightly in this region for best results. For straight wings, clustering is only needed near the wingtips [33]. Cosine clustering was done by examining the entire span to allow for cosine clustering at the tips

only instead of the tips and the root. For example, if the desired number of twist locations for the semispan were 10, the spanwise location (z/b) to apply the twist would be calculated using

$$\Delta\theta = \frac{\pi}{(N*2)-2} \tag{4.2}$$

where the term N is the desired number of twist location for the semispan and the term $((N*2)-2)$, accounts for the total number of twist locations for the entire wing. So for 10 twist locations per semispan, $((N*2)-2{=}18)$, so that the values between ($\cos(10*\Delta\theta)$-$\cos(18*\Delta\theta)$) correspond to the correct spanwise location (z/b).

To find the optimum number of twist locations, optimization of the wing outside of ground effect was done with the amount of twist control points varying between 1-20. Those results are shown in Figures 4.2 and 4.3.

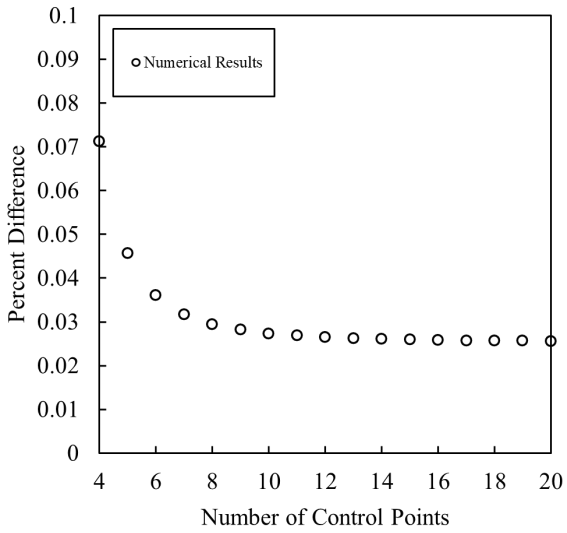

Fig. 4.2: Percent difference between the minimum induced drag found using between 4-20 control points to optimize the solution and the analytical solution found using equation 1.24 for a rectangular wing of aspect ratio 8 at a lift coefficient of 0.5.

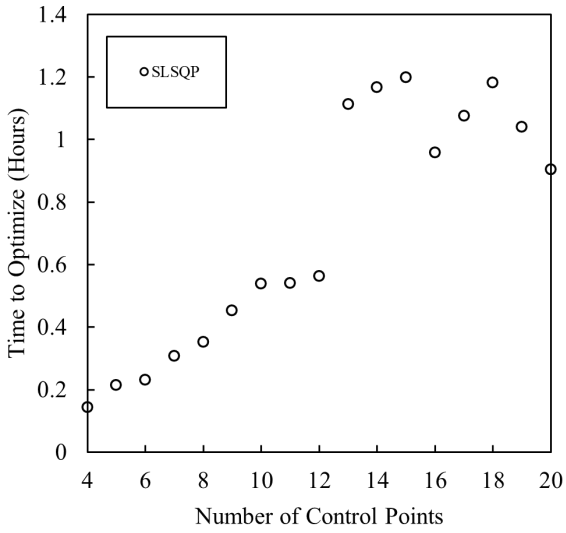

Fig. 4.3: Time required for SLSQP optimization method to converge and minimize the induced drag on a rectangular wing of aspect ratio 8 at a lift coefficient of 0.5.

By examining Figure 4.2 we see that the percent difference between the numerical and analytic solution begins to level off when 10 control points are used. By examining 4.3, we notice that there is a significant jump in the time required to converge when 13 control points is reached. Because the percent difference between the numerical and analytic solution when using between 10-20, the number of control points that converged in the least amount of time was selected to allow for more variations of wing planforms to be studied. For this work, the number of twist locations used is 10.

CHAPTER 5

RESULTS

The rectangular wing used in this work had the parameters shown in Table 5.1. A section lift slope from thin-airfoil theory of 2π was used, and a symmetric airfoil was assumed $\alpha_{L0} = 0$.

Table 5.1: Rectangular Wing Parameters

Parameter	Value
Nodes per Semispan	100
Twist Control Points	10
Max Iterations	1000
Tolerance	$1e^{-9}$
R_A	8.0
R_T	1.0
Area ft^2	8.0
C_L	0.5
$\tilde{C}_{L,\alpha}$	2π
α_{L0}	0

With the overall goal of minimizing the induced drag on any given planform in ground effect, it is necessary to understand how the lift and induced drag distributions change as the wing approaches the ground. To better understand this, it is helpful to define section lift and induced drag coefficients that allow us to see how the distributions vary with respect to the local chord at any spanwise location as well as how the distribution varies along the span.

Because $\hat{x}$ is defined in the direction of drag and $\hat{z}$ is defined in the direction of lift in MachUpX, the section lift and induced drag coefficients that are scaled by the local chord

are $\tilde{C}_L$ are $\tilde{C}_{Di}$ and are defined by

$$\tilde{C}_L = \frac{-\tilde{F}_{\hat{z}}}{\frac{1}{2}\rho V^2 c} \tag{5.1}$$

$$\tilde{C}_{Di} = \frac{-\tilde{F}_{\hat{x}}}{\frac{1}{2}\rho V^2 c} \tag{5.2}$$

where $\tilde{L}$ is the lift at a specific spanwise location along the wing, ρ and V^2 are the air density and freestream velocity, c is the local chord length of the spanwise section, and R_A is the wing aspect ratio.

Because $\tilde{C}_L$ are $\tilde{C}_{Di}$ are scaled by the local chord, they do not show how the dimensional distribution varies along the span. For this reason, we will use additional variables for the lift and induced drag coefficients that are normalized by the wingspan given by

$$\hat{C}_L = \tilde{C}_L \frac{c(z)}{b} \tag{5.3}$$

and

$$\hat{C}_{Di} = \tilde{C}_{Di} \frac{c(z)}{b} \tag{5.4}$$

Figures 5.1, 5.2, 5.4, and 5.5 contain results using MachUpX to determine the section lift and drag coefficients in and out of ground effect for an untwisted rectangular wing, an optimally twisted rectangular wing, a rectangular wing twisted using Eq. 1.29 , as well as an elliptic wing. All results were obtained with the wings having a total lift coefficient of 0.5 ($C_L = 0.5$) with identical wing areas and aspect ratios.

In Figure 5.1a and 5.1b, a few specific things are important. When comparing the optimal solution in ground effect, shown by the solid green line in Fig. 5.1a and 5.1b, with the other solutions in ground effect, we notice that the lift is shifted inboard towards the root of the wing.

The shift in lift distribution is particularly noticeable for an elliptic wing. By examining the blue lines in Fig. 5.1a, we note that the lift distribution is nearly a straight line out of ground effect at a lift coefficient of 0.5 across the semispan. In ground effect, the lift

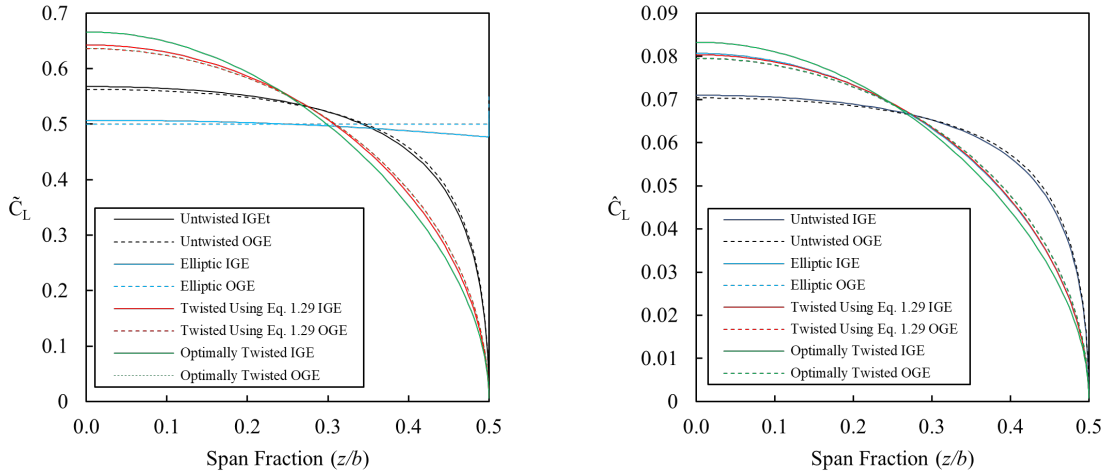

(a) (b)

Fig. 5.1: Comparison of results predicted by MachUpX for the (a) lift distribution and (b) normalized lift distribution of an untwisted rectangular wing, elliptic wing, rectangular wing with an elliptic twist distribution, and an optimally twisted rectangular wing in and out of ground effect at a lift coefficient of 0.5.

distribution shifts inboard so that the lift is higher at the root and less at the tip.

In previous sections, we established that Phillip's twist distribution equation, Eq. 1.29, which produces an elliptic lift distribution, is the optimum solution out of ground effect. This is validated by examining the results in Fig. 5.1b, which contains results for the lift coefficient normalized by chord length. Because this work studied a rectangular wing, the shape of the data for all non-elliptic remains the same. In contrast, the elliptic lift distribution goes from a nearly straight line in Fig. 5.1a to the elliptic distribution shown in Fig. 5.1b.

In Fig 5.1b, note that all solutions obtained out of ground effect lie on each other, other than for the untwisted wing, which further validates that Phillip's solution produces the minimum induced drag.

Like Figure 5.1a and 5.1b, the only difference between Figure 5.2a and 5.2b is that Fig. 5.2b is normalized by the section chord, which allows us to visualize how twisting the wing manipulates the lift distribution to match that of an elliptic wing.

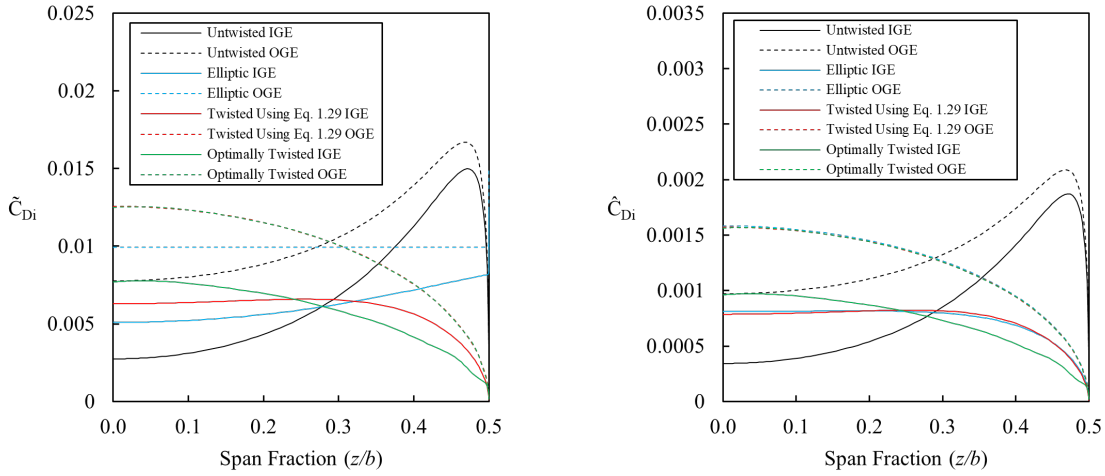

(a) (b)

Fig. 5.2: Comparison of results predicted by MachUpX for the (a) induced drag distribution and (b) normalized induced drag distribution of an untwisted rectangular wing, elliptic wing, rectangular wing with an elliptic twist distribution, and an optimally twisted rectangular wing in and out of ground effect at a lift coefficient of 0.5.

In Fig. 5.2a, one thing of note that can be gleaned from this figure is that out of ground effect, the induced drag is nearly the same across the semispan for an elliptic wing. In ground effect, the induced drag is reduced across the entire semispan, with the most significant reduction occurring at the root of the wing. This occurred for all wings tested in this work; when the wing is in ground effect, the induced drag is reduced across the entire span, with the most significant reduction in drag occurring at the root.

Like Fig. 5.1b, the results in Fig. 5.2b for the test cases out of ground effect lie on each other, except for the untwisted results. These results further validate that Phillip's method, which twists a wing to produce the elliptic lift distribution, is the distribution that minimizes induced drag out of ground effect. However, in ground effect, the optimum solution is different in that it increases the induced drag toward the root and reduces the induced drag toward the tip.

Figure 5.3a shows the total amount of wing twist, aerodynamic plus geometric, for an optimally twisted rectangular wing as it gets closer to the ground and compares it with the twist for a rectangular wing twisted using Eq. 1.29 out of ground effect. Because the

effect the ground has increases the closer the wing gets, we notice that for values of h/b between 1.0 and 2.0, the total twist calculated using the optimization routine matches the twist calculated using Eq. 1.29. At $h/b = 0.5$, we see a slight deviation from the optimal solutions out of ground effect and begin to see the effect of the ground. However, at h/b= 0.5, the twist distribution profile is nearly identical to Phillips, with the only difference being the angle of attack being slightly lower. As we get closer to the ground, in the results calculated at $h/b = 0.25$ and $h/b = 0.125$, the overall twist distribution begins to differ more and more from Phillip's solution. As the wing approaches the ground, the optimal solution predicts an increase in total twist at the root of the wing and a decrease in total twist as we go outboard towards the wing tip.

Figure 5.3b shows the normalized twist distribution for the wings shown in Fig. 5.3a. Because the induced drag at the wing tip approaches zero, the data is skewed if we normalize it by the total length of the semispan. To counter this, the results were normalized with respect to 98% of the semispan, which cleaned up discrepancies in the data presented in the wing tip. As seen in Fig. 5.3b, ground effect does not have much effect for values of h/b between 1.0 and 2.0. The normalized twist distributions at these heights above ground are nearly identical to that predicted by Eq. 1.29 out of ground effect. At $h/b = 0.5$, the twist distribution begins to differ from Phillip's solution, with more significant differences occurring at $h/b = 0.25$ and $h/b = 0.125$.

Figures 5.4a and 5.4b show the solutions for the lift distribution of an optimally twisted rectangular wing, represented with solid lines, as it approaches the ground. Fig. 5.4a compares the lift distribution of the optimally twisted wing to the lift distribution of an untwisted identical rectangular wing with solutions represented with dashed lines. Fig. 5.4b compares the lift distributions of the optimally twisted wing to the lift distribution of an identical rectangular wing twisted using Eq. 1.29 with solutions represented with dashed lines. From Figures 5.4a and 5.4b, we notice that the lift distributions are nearly identical even as the wing approaches the ground. Consequently, we learn that the lift distribution does not significantly change as the wing approaches the ground for untwisted rectangular

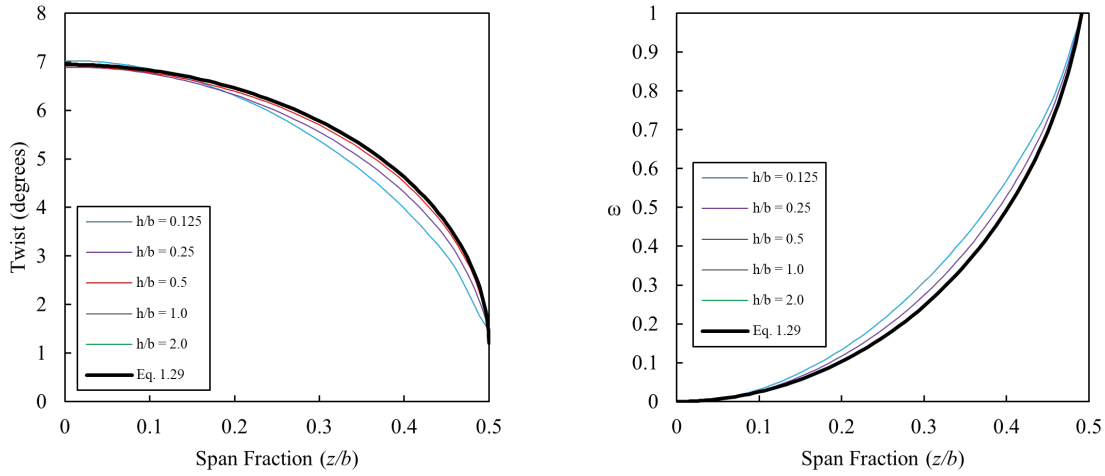

(a) (b)

Fig. 5.3: Comparison of results for the (a) total amount of wing twist, (Geometric wing twist + α_{root}), and (b) normalized wing twist for an optimally twisted rectangular wing of aspect ratio 8 at a lift coefficient of 0.5 at varying heights above ground.

wings and rectangular wings twisted using Eq. 1.29. However, at a height above ground of 0.125 ($h/b = 0.125$), the optimal solution alters the lift distribution and shifts the lift inboard.

Figures 5.5a and 5.5b show the solutions for the induced drag distribution of an optimally twisted rectangular wing, represented with solid lines, as it approaches the ground. Fig. 5.5a compares the induced drag distribution of the optimally twisted wing to the induced drag distribution of an untwisted identical rectangular wing with solutions represented with dashed lines. Fig. 5.5b compares the induced drag distribution of the optimally twisted wing to the induced drag distribution of an identical rectangular wing twisted using Eq. 1.29 with solutions represented with dashed lines. From Figures 5.5a and 5.5b, we notice that unlike the lift distributions in 5.4a and 5.4b, the induced drag distributions change significantly as the wing approaches the ground.

In the comparison of lift distributions shown in Fig. 5.4b, where the difference between the optimal solution and the solution obtained using the twist distribution from Eq. 1.29 was minute, Fig. 5.5b shows that the induced drag distribution is significantly reduced at the root as the wing approaches the ground in comparison to the induced drag distribution

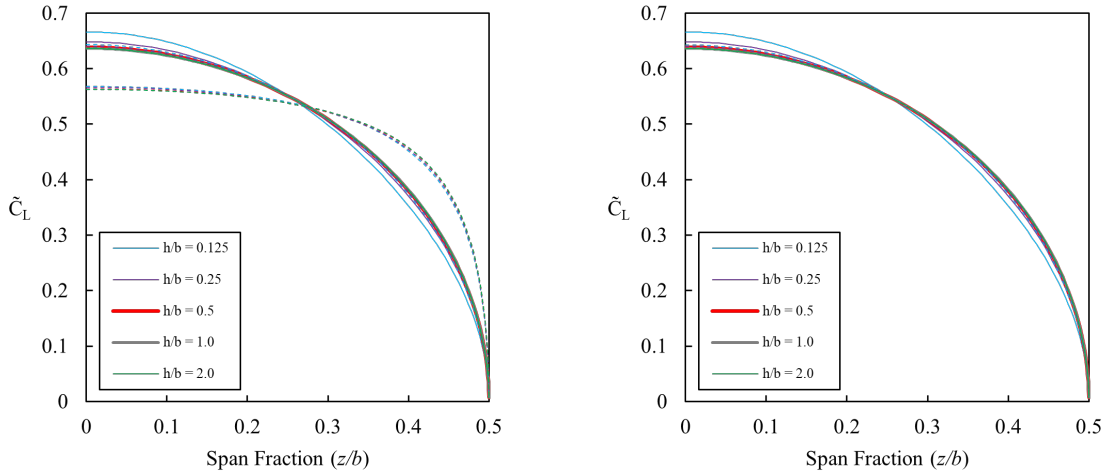

(a) Dashed lines represent the results calculated using the untwisted wing.

(b) Dashed lines represent the results calculated using Eq. 1.29 to twist the wing.

Fig. 5.4: Comparison of results predicted by MachUpX for the lift distribution for a rectangular wing of aspect ratio 8 at a lift coefficient of 0.5 at varying heights above ground. Solid lines represent the results calculated using the optimally twisted wing.

for a wing twisted using Eq. 1.29. Although the induced drag distribution is altered, the overall induced drag is nearly identical.

Figure 5.6 shows the comparison of the induced drag calculated at various heights above ground for the optimally twisted wing, untwisted identical rectangular wing, and a rectangular wing twisted using Eq. 1.29. From Fig. 5.6, note that the induced drag is decreased as the wing approaches the ground, regardless of wing twist.

Figure 5.7 compares the percent reduction in induced drag caused by twisting the wing to the induced drag for the untwisted rectangular wing. As the wing approaches the ground, the optimal solution mirrors the solution predicted by Phillip's using Eq. 1.29. There is a slight improvement in induced drag reduction as the wing is very close to the ground where $h/b = 0.125$. However, the improvement is less than 1%.

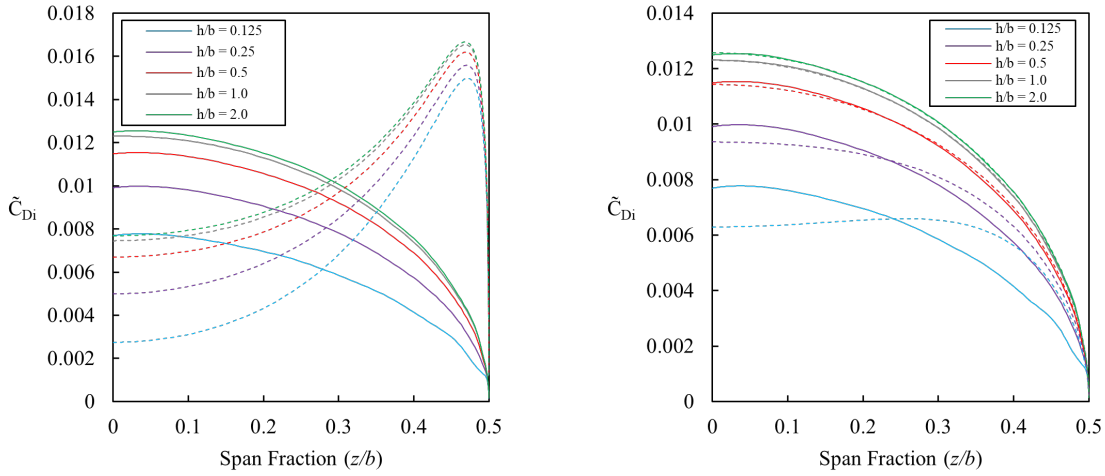

(a) Dashed lines represent the results calculated using the untwisted wing.

(b) Dashed lines represent the results calculated using Eq. 1.29 to twist the wing.

Fig. 5.5: Comparison of results predicted by MachUpX for the induced drag distribution for a rectangular wing of aspect ratio 8 at a lift coefficient of 0.5 at varying heights above ground. Solid lines represent the results calculated using the optimally twisted wing.

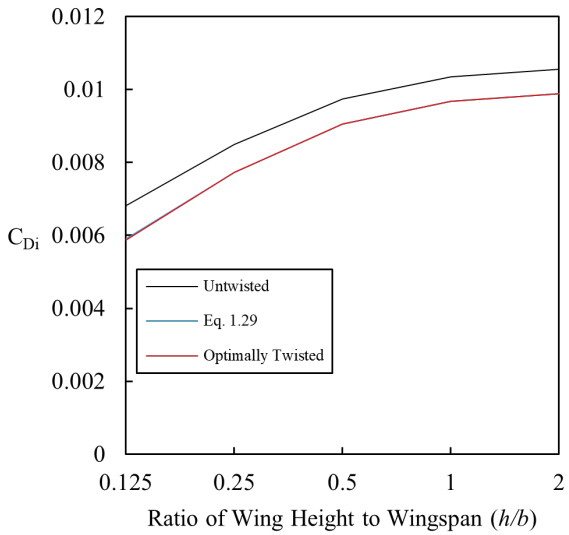

Fig. 5.6: Comparison of results predicted by MachUpX for the total induced drag of an untwisted rectangular wing, rectangular wing with an elliptic twist distribution, and an optimally twisted rectangular wing at varying heights above ground at a lift coefficient of 0.5.

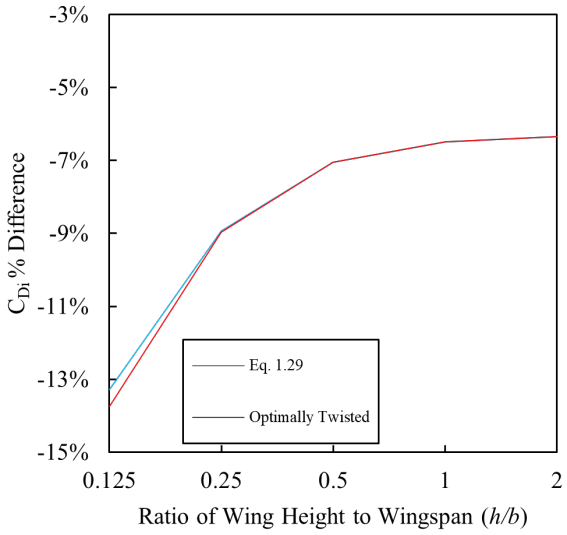

Fig. 5.7: Comparison of percent difference in total induced drag of a rectangular wing with an elliptic twist distribution and an optimally twisted rectangular wing, with that of an untwisted rectangular wing at varying heights above ground at a lift coefficient of 0.5.

Although the induced drag distribution is different between the optimally twisted wing and the wing twisted using Eq. 1.29, as shown in Fig. 5.5b, the induced drag for both methods is nearly identical even as the wing gets closer to the ground. These results are shown in Table 5.2.

Table 5.2: Comparison of Total Induced Drag at Various Heights Above Ground

h/b	Optimum	Eq. 1.29	Untwisted
2.0	0.009876886	0.009876784	0.010546807
1.0	0.009675912	0.009675798	0.010347736
0.5	0.009055958	0.009055925	0.009743482
0.25	0.007725199	0.007729060	0.008486995
0.125	0.005871678	0.005903083	0.006807570

Therefore, although the induced drag distribution is altered to be reduced at the root and shifted outboard toward the tip, the overall induced drag is still very nearly the same. This is also shown by calculating the percent reduction in induced drag. These results are given in Table 5.3.

Table 5.3: Percent Reduction in Induced Drag Comparison Between Optimum Solution and Eq. 1.29

h/b	Optimum	Eq. 1.29
2.0	-6.35%	-6.35%
1.0	-6.49%	-6.49%
0.5	-7.06%	-7.06%
0.25	-8.98%	-8.93%
0.125	-13.75%	-13.29%

CHAPTER 6
SUMMARY AND CONCLUSION

Significant research has been done into methods to optimize specific aerodynamic characteristics of aircraft, such as the minimization of induced drag. Research by Prandtl showed that the elliptic lift distribution minimizes induced drag on a single straight wing with a given wingspan and desired lift [1–3]. However, elliptic wings can be difficult and costly to manufacture [4], which has led to other methods of achieving the elliptic lift distribution through manipulation of the wing through twist.

A closed-form analytic solution published by Phillips [6] shows that there is a symmetric baseline twist distribution, amount, and angle of attack for any given wing planform that minimizes the induced drag at a prescribed lift coefficient and zero roll and yaw [4–7]. However, these solutions are for a wing outside of ground effect. Most fixed-wing aircraft spend time close to the ground during takeoff and landing, affecting the aerodynamic characteristics of the aircraft's lifting surface, typically resulting in an increase in lift and a decrease in induced drag [8].

From Fig. 1.1, we see that as the wing gets closer to the ground, the lift and induced drag deviate further from their values at the same lift coefficient outside of ground effect. Because we know that the lift and drag change as we approach the ground, we expected the lift and induced drag distributions to differ for a wing in ground effect compared to a wing out of ground effect. For that reason, this work sought the twist distribution that would minimize the induced drag on a rectangular wing in ground effect.

Results for the optimum twist distributions and resulting induced drag were computed numerically using a modern numerical lifting-line algorithm implemented through the Python package MachUpX [31, 34]. Ground effect was modeled by replacing the ground's

surface with an image of the aircraft, positioned and oriented as if it were reflected in the ground's surface as shown by Fig. 3.1.

The optimization routine was performed using Python's SciPy library and the Sequential Least Squares Programming (SLSQP) minimization algorithm was implemented. Results obtained using the SLSQP method are not guaranteed to be the global minimum solution. However, results obtained by initializing the wing twist to values above and below the expected results converged to a solution within 1% as shown in Fig.3.2.

A grid resolution study was performed to determine the optimum number of nodes to be used in the lifting-line algorithm and the number of twist locations to be used in the SLSQP optimization routine. Based on this study, 100 nodes per semispan and 10 control points were chosen. The control point twist locations were cosine clustered to allow for more twist control points toward the tip of the wing and less toward the root.

Results in Figures 5.1 and 5.2 validated that the elliptic lift distribution is the optimum lift distribution out of ground effect that minimizes induced drag. Additionally, Fig. 5.4 shows that as the wing approaches the ground the lift distribution is shifted inboard but is not significantly altered. It was found that ground effect had a much more significant effect on the induced drag distribution as seen in Figures 5.2 and 5.5. The optimal solution moves the induced drag inboard compared to the solution found by twisting the wing using Eq. 1.29.

From Fig. 5.3, we noticed that the total twist and normalized twist distribution approaches the solution predicted by Eq. 1.29 as we get further from the ground. As the wing approaches the ground, that twist distribution has less curvature between the root and the tip and approaches a linear distribution. While the induced drag distribution was altered using the optimization routine, the actual reduction in induced drag compared to the results using Eq. 1.29 was small which can be seen in Table 5.3.

While the solutions here showed that for a rectangular wing, Eq. 1.29 provides nearly identical results in ground effect, the solutions included here provide insight into how the lift and induced drag distribution change as the wing approach the ground. These results

can be helpful in future studies that seek to further minimize the induced drag in ground effect.

One interesting note found by examining the figures in this work was that ground effect shifts the lift inboard and the induced drag outboard. In nearly all results, the solution in ground effect crossed the solution out of ground effect at a spanwise location between 0.25 and 0.3. One possible future research area is examining why the ground effect solution crossed at this location. Future work could also study the effects of dihedral or wing taper in ground effect.

REFERENCES

[1] PRANDTL, L., "TragflÃ¼geltheorie. I. Mitteilung," *Nachrichten von der Gesellschaft der Wissenschaften zu GÃ¶ttingen, Mathematisch-Physikalische Klasse*, Vol. 1918, 1918, pp. 451–477.

[2] Prandtl, L., "Applications of modern hydrodynamics to aeronautics. NACATR 116," *NACA Technical Report*, Vol. 121, 1921.

[3] Hunsaker, D. F. and Phillips, W., "Ludwig Prandtlâs 1933 Paper Concerning Wings for Minimum Induced Drag, Translation and Commentary," *AIAA Scitech 2020 Forum*, American Institute of Aeronautics and Astronautics, _eprint: https://arc.aiaa.org/doi/pdf/10.2514/6.2020-0644.

[4] Phillips, W. F., "Incompressible Flow over Finite Wings," *Mechanics of Flight*, chap. 1, John Wiley Sons, Inc., 2nd ed., 2010, pp. 46–94.

[5] Phillips, W., Alley, N., and Goodrich, W., "Lifting-line analysis of roll control and variable twist," *Journal of aircraft*, Vol. 41, No. 5, 2004, pp. 1169–1176.

[6] Phillips, W., "Lifting-line analysis for twisted wings and washout-optimized wings," *Journal of aircraft*, Vol. 41, No. 1, 2004, pp. 128–136.

[7] Phillips, W. and Hunsaker, D., "Designing wing twist or planform distributions for specified lift distributions," *Journal of Aircraft*, Vol. 56, No. 2, 2019, pp. 847–849.

[8] Phillips, W. F. and Hunsaker, D. F., "Lifting-line predictions for induced drag and lift in ground effect," *Journal of Aircraft*, Vol. 50, No. 4, 2013, pp. 1226–1233.

[9] Rozhdestvensky, K. V., "Wing-in-ground effect vehicles," *Progress in aerospace sciences*, Vol. 42, No. 3, 2006, pp. 211–283.

[10] Phillips, W. F., "Takeoff and Landing Performance," *Mechanics of Flight*, chap. 3, John Wiley Sons, Inc., 2nd ed., 2010, pp. 337–353.

[11] Phillips, W. F., "Ground Effect, Elevator Sizing, and CG Limits," *Mechanics of Flight*, chap. 6, John Wiley Sons, Inc., 2nd ed., 2010, pp. 646–661.

[12] McGowan, A.-M. R., Washburn, A. E., Horta, L. G., Bryant, R. G., Cox, D. E., Siochi, E. J., Padula, S. L., and Holloway, N. M., "Recent results from NASA's morphing project," *Smart structures and materials 2002: industrial and commercial applications of smart structures technologies*, Vol. 4698, SPIE, 2002, pp. 97–111.

[13] Kota, S., Flick, P., and Collier, F. S., "Flight testing of flexfloiltm adaptive compliant trailing edge," *54th AIAA Aerospace Sciences Meeting*, 2016, p. 0036.

[14] Kota, S. and Martins, J., "Flexfloil shape adaptive control surfaces-flight test and numerical results," *Proceedings of 31st Congress of the International Council of the Aeronautical Sciences (ICAS 2018), Belo Horizonte, Brazil*, 2018, p. 1709.

[15] Hunsaker, D. F., Phillips, W. F., and Joo, J. J., "Aerodynamic shape optimization of morphing wings at multiple flight conditions," *55th AIAA aerospace sciences meeting*, 2017, p. 1420.

[16] Kutta, W., "Auftriebskräfte in strömenden Flüssigkeiten," *Illustrierte Aeronautische Mitteilungen*, Vol. 6, No. 133, 1902, pp. 133–135.

[17] Joukowski, N., "Sur les Tourbillons Adjionts," *Traraux de la Section Physique de la Societé Imperiale des Amis des Sciences Naturales*, Vol. 13, No. 2, 1906, pp. 261–284.

[18] Phillips, W. F., "Analytical decomposition of wing roll and flapping using lifting-line theory," *Journal of Aircraft*, Vol. 51, No. 3, 2014, pp. 761–778.

[19] Phillips, W. F. and Alley, N. R., "Predicting maximum lift coefficient for twisted wings using lifting-line theory," *Journal of aircraft*, Vol. 44, No. 3, 2007, pp. 898–910.

[20] Phillips, W. F., Fugal, S. R., and Spall, R. E., "Minimizing induced drag with wing twist, computational-fluid-dynamics validation," *Journal of Aircraft*, Vol. 43, No. 2, 2006, pp. 437–444.

[21] Phillips, W. F., "New twist on an old wing theory," *Aerospace America*, Vol. 43, No. 1, 2005, pp. 27–30.

[22] Phillips, W., "Lifting-line analysis for twisted wings and washout-optimized wings," *Journal of aircraft*, Vol. 41, No. 1, 2004, pp. 128–136.

[23] Glauert, H., "The Monoplane Aerofoil, The Elements of Aerofoil and Airscrew Theory, Cambridge Univ. Press, Cambridge, UK, 1926, pp. 137-155," .

[24] Phillips, W. F., Hunsaker, D. F., and Taylor, J. D., "Minimising induced drag with weight distribution, lift distribution, wingspan, and wing-structure weight," *The Aeronautical Journal*, Vol. 124, No. 1278, 2020, pp. 1208–1235.

[25] Phillips, W., Hunsaker, D., and Joo, J., "Minimizing induced drag with lift distribution and wingspan," *Journal of Aircraft*, Vol. 56, No. 2, 2019, pp. 431–441.

[26] Hoerner, S. and Borst, H., "Lift of Airplane Configurations," *Fluid Dynamic Lift, Hoerner Fluid Dynamics, Bricktown, NJ*, 1975, pp. 20–1.

[27] McCormick, B. W., *Aerodynamics, aeronautics and flight mechanics*, Wiley, 1979.

[28] Torenbeek, E., "Ground Effects," *Synthesis of Subsonic Airplane Design, Delft University Press, Delft, The Netherlands*, 1982, pp. 551–554.

[29] McCormick, B. W., *Aerodynamics, Aeronautics, and Flight Mechanics*, John Wiley Sons, Inc., 2nd ed., 1995.

[30] Bertin, J., "Incompressible Flow About Wings of Finite Span," *Aerodynamics for Engineers, 4th ed., Prentice-Hall, Upper Saddle River, New Jersey*, 2002, pp. 230–302.

[31] Phillips, W. F. and Snyder, D., "Modern adaptation of Prandtl's classic lifting-line theory," *Journal of Aircraft*, Vol. 37, No. 4, 2000, pp. 662–670.

[32] Anderson, J., "Fundamentals of Aerodynamics, 36 McGraw-Hill education," *New York*, 2010.

[33] Phillips, W. F., "Flow Over Multiple Lifting Surfaces," *Mechanics of Flight*, chap. 1, John Wiley Sons, Inc., 2nd ed., 2010, pp. 94–107.

[34] Reid, J. T. and Hunsaker, D. F., "A General Approach to Lifting-Line Theory, Applied to Wings with Sweep," *AIAA Scitech 2020 Forum*, American Institute of Aeronautics and Astronautics, Jan 2020.

[35] Weber, J., Brebner, G., and Kuchemann, D., "Low-Speed Tests on 45-deg Swept-back Wings Parts I and II," 1951.

[36] Goates, C. D. and Hunsaker, D. F., "Practical Implementation of a General Numerical Lifting-Line Method," *AIAA SciTech 2021 Forum*, 2021, p. 0118.

[37] Fleming, P. A., Stanley, A. P., Bay, C. J., King, J., Simley, E., Doekemeijer, B. M., and Mudafort, R., "Serial-Refine Method for Fast Wake-Steering Yaw Optimization," *Journal of Physics: Conference Series*, Vol. 2265, IOP Publishing, 2022, p. 032109.

[38] Kraft, D., "A software package for sequential quadratic programming," *Forschungsbericht- Deutsche Forschungs- und Versuchsanstalt fur Luft- und Raumfahrt*, 1988.

[39] Thurgood, J., "Aircraft Input Files for Pylot and MachUpX," 2021.

APPENDICES

APPENDIX A

CODE FOR SCENE OBJECT

This appendix contains the JSON input file describing the aircraft scene and state of the aircraft.

```
{
    "tag" : "Example input file using a rectangular wing",
    "run" : {
        "display_wireframe" : {
            "show_legend" : true
        },
        "solve_forces" : {
            "non_dimensional" : true
        },
        "pitch_trim" : {
            "set_state_to_trim" : true
        },
        "derivatives" : {}
    },
    "solver" : {
        "type" : "nonlinear",
        "convergence" : 1e-9,
        "relaxation" : 1.0
    },
    "units" : "English",
    "scene" : {
        "atmosphere" : {},
        "aircraft" : {
```

```
            "traditional_airplane" : {
                "file" : "IGE_rewritten_wing_input.json",
                "state" : {
                    "velocity" : 100,
                    "alpha" : 0.0,
                    "beta" : 0.0
                },
                "control_state" : {
                    "elevator" : 0.0,
                    "rudder" : 0.0,
                    "aileron" : 0.0
                }
            }
        }
    }
}
```

APPENDIX B

CODE FOR AIRCRAFT OBJECT

This appendix contains the JSON input file describing the aircraft and geometry in ground effect at a height above ground ratio of 0.125 (h/b=0.125) The wing is initialized at uniform twist values of 0.0 degrees.

```
{
  "CG": [0,0,0],
  "weight": 100.0,
  "reference": {
     "area": 8.0,
     "longitudinal_length": 1.0,
     "lateral_length": 8.0
  },
  "airfoils": {
    "Thin_Airfoil": {
      "type": "linear",
      "aL0": 0.0,
      "CLa": 6.28318530717959,
      "CmL0": 0.0,
      "Cma": 0.0,
      "CD0": 0.0,
      "CD1": 0.0,
      "CD2": 0.0,
      "CL_max": 1.4}
  },
  "wings": {
    "main_wing": {
```

```
  "ID": 1,
  "side": "both",
  "is_main": true,
  "connect_to": {
    "location": "root",
    "dz": -1.0
  },
  "semispan": 4.0,
  "airfoil": "Thin_Airfoil",
  "twist": [
    [0.0,0.0],
    [0.17364817766693,0.0],
    [0.342020143325669,0.0],
    [0.5,0.0],
    [0.642787609686539,0.0],
    [0.766044443118978,0.0],
    [0.866025403784438,0.0],
    [0.939692620785908,0.0],
    [0.984807753012208,0.0],
    [1.0,0.0]],
  "chord": [
    [0.0,1.0],
    [1.0,1.0]],
  "grid": {
    "N": 100
  }
},
"ground_effect_wing": {
  "ID": 2,
  "side": "both",
  "is_main": false,
  "connect_to": {
```

```
      "location": "root",
      "dz": 1.0
    },
    "semispan": 4.0,
    "airfoil": "Thin_Airfoil",
    "twist": [
      [0.0,0.0],
      [0.17364817766693,0.0],
      [0.342020143325669,0.0],
      [0.5,0.0],
      [0.642787609686539,0.0],
      [0.766044443118978,0.0],
      [0.866025403784438,0.0],
      [0.939692620785908,0.0],
      [0.984807753012208,0.0],
      [1.0,0.0]],
    "chord": [
      [0.0,1.0],
      [1.0,1.0]],
    "grid": {
      "N": 100
    }
  }
 }
}
```

APPENDIX C
CODE FOR AIRCRAFT OBJECT

This appendix contains the JSON input file describing the aircraft and geometry in ground effect at a height above ground ratio of 0.125 (h/b=0.125) The wing is initialized at uniform twist values of 8.0 degrees.

```
{
  "CG": [0,0,0],
  "weight": 100.0,
  "reference": {
     "area": 8.0,
     "longitudinal_length": 1.0,
     "lateral_length": 8.0
  },
  "airfoils": {
    "Thin_Airfoil": {
      "type": "linear",
      "aL0": 0.0,
      "CLa": 6.28318530717959,
      "CmL0": 0.0,
      "Cma": 0.0,
      "CD0": 0.0,
      "CD1": 0.0,
      "CD2": 0.0,
      "CL_max": 1.4}
  },
  "wings": {
    "main_wing": {
```

```
  "ID": 1,
  "side": "both",
  "is_main": true,
  "connect_to": {
    "location": "root",
    "dz": -1.0
  },
  "semispan": 4.0,
  "airfoil": "Thin_Airfoil",
  "twist": [
    [0.0,8.0],
    [0.17364817766693,8.0],
    [0.342020143325669,8.0],
    [0.5,8.0],
    [0.642787609686539,8.0],
    [0.766044443118978,8.0],
    [0.866025403784438,8.0],
    [0.939692620785908,8.0],
    [0.984807753012208,8.0],
    [1.0,8.0]],
  "chord": [
    [0.0,1.0],
    [1.0,1.0]],
  "grid": {
    "N": 100
  }
},
"ground_effect_wing": {
  "ID": 2,
  "side": "both",
  "is_main": false,
  "connect_to": {
```

```
      "location": "root",
      "dz": 1.0
    },
    "semispan": 4.0,
    "airfoil": "Thin_Airfoil",
    "twist": [
      [0.0,-8.0],
      [0.17364817766693,-8.0],
      [0.342020143325669,-8.0],
      [0.5,-8.0],
      [0.642787609686539,-8.0],
      [0.766044443118978,-8.0],
      [0.866025403784438,-8.0],
      [0.939692620785908,-8.0],
      [0.984807753012208,-8.0],
      [1.0,-8.0]],
    "chord": [
      [0.0,1.0],
      [1.0,1.0]],
    "grid": {
      "N": 100
    }
   }
  }
}
```

APPENDIX D
CODE FOR AIRCRAFT OBJECT

This appendix contains the JSON input file describing the aircraft and geometry in ground effect at a height above ground ratio of 0.125 (h/b=0.125) The wing is initialized at twist values according to Eq. 1.29.

```
{
  "CG": [0,0,0],
  "weight": 100.0,
  "reference": {
     "area": 8.0,
     "longitudinal_length": 1.0,
     "lateral_length": 8.0
  },
  "airfoils": {
    "Thin_Airfoil": {
      "type": "linear",
      "aL0": 0.0,
      "CLa": 6.28318530717959,
      "CmL0": 0.0,
      "Cma": 0.0,
      "CD0": 0.0,
      "CD1": 0.0,
      "CD2": 0.0,
      "CL_max": 1.4}
  },
  "wings": {
    "main_wing": {
```

```
  "ID": 1,
  "side": "both",
  "is_main": true,
  "connect_to": {
    "location": "root",
    "dz": -1.0
  },
  "semispan": 4.0,
  "airfoil": "Thin_Airfoil",
  "twist": [
    [0.0,6.70676662919402],
    [0.17364817766693,6.61857143919401],
    [0.342020143325669,6.35666563619402],
    [0.5,5.92900709419402],
    [0.642787609686539,5.34859000319401],
    [0.766044443118978,4.63305004219402],
    [0.866025403784438,3.80412853019401],
    [0.939692620785908,2.88701182819401],
    [0.984807753012208,1.90956606419401],
    [1.0,0.901490431194027]],
  "chord": [
    [0.0,1.0],
    [1.0,1.0]],
  "grid": {
    "N": 100
  }
},
"ground_effect_wing": {
  "ID": 2,
  "side": "both",
  "is_main": false,
  "connect_to": {
```

```
      "location": "root",
      "dz": 1.0
    },
    "semispan": 4.0,
    "airfoil": "Thin_Airfoil",
    "twist": [
      [0.0,-6.70676662919402],
      [0.17364817766693,-6.61857143919401],
      [0.342020143325669,-6.35666563619402],
      [0.5,-5.92900709419402],
      [0.642787609686539,-5.34859000319401],
      [0.766044443118978,-4.63305004219402],
      [0.866025403784438,-3.80412853019401],
      [0.939692620785908,-2.88701182819401],
      [0.984807753012208,-1.90956606419401],
      [1.0,-0.901490431194027]],
    "chord": [
      [0.0,1.0],
      [1.0,1.0]],
    "grid": {
      "N": 100
    }
   }
  }
}
```

APPENDIX E

MAIN PYTHON CODE

This appendix contains the main body of the Python code used in this work

```
# -*- coding: utf-8 -*-
"""
Created on Tue Oct 25 16:30:00 2022

@author: Kyler Church
"""
import json
import numpy as np
import matplotlib.pyplot as plt
import scipy.optimize as sopt
import MachUpX as MX

def solve(initial_twist_array, target_CL):
    """
    Parameter: list containing twist values at each twist control point, as well
        as the
    desired lift coefficient
    Returns: the amount of twist at each node, the difference between the target
        lift and
    the actual lift coefficient, as well as the minimized induced drag
    """
    result = sopt.minimize(myCD, initial_twist_array, method='SLSQP', jac='3-point
        ',
    constraints={'type' : 'eq', 'fun' : myCL}, tol= 1e-08, options={'eps':
```

```
    1.4901161193847656e-04, 'maxiter': 1000,'disp':True})

    CL_residual = myCL(result.x)
    CDi = myCD(result.x)
    twist = result.x

    return twist, CL_residual, CDi

def myCD(twist_array):
    """
    Parameter: list containing twist values at each twist control point
    Returns: the total induced drag on the wing, this is the function that
        optimization
    routine is minimizing. Multiplying the returned value by 100 makes the
        equality
    constraint and the minimized value have the same order of magnitude which
        helps with
    convergence and better results.
    """
    CL_total_main, CD_total_main, z_b, twist, right_section_CL, right_section_CDi,
    right_section_CL_FZ, right_section_CDi_FX = run_case(twist_array)

    return CD_total_main*100

def myCL(twist_array):
    """
    Parameter: list containing twist values at each twist control point
    Returns: the difference between the target lift coefficient and the actual
        coefficient,
    optimization routine ensures this returns 0 so that the wing is at a lift
        coefficient
    of 0.5
```

```
    """
    target_CL = 0.5
    CL_total_main, CD_total_main, z_b, twist, right_section_CL, right_section_CDi,
    right_section_CL_FZ, right_section_CDi_FX = run_case(twist_array)

    return CL_total_main - target_CL

def mydist(twist_array):
    """
    Parameter: list containing twist values at each twist control point
    Returns: total lift and induced drag, lists for the spanwise fraction, twist
        value, lift
    and drag coefficients, and forces acting in the axial and normal directions at
         each
    nodal location
    """
    CL_total_main, CD_total_main, z_b, twist, right_section_CL, right_section_CDi,
    right_section_CL_FZ, right_section_CDi_FX = run_case(twist_array)

    return CL_total_main, CD_total_main,z_b, twist, right_section_CL,
        right_section_CDi,
    right_section_CL_FZ, right_section_CDi_FX

def run_case(twist_distribution):
    """
    Parameter: twist distribution specified in "is_main"
    Returns: total lift and induced drag, lists for the spanwise fraction, twist
        value, lift
    and drag coefficients, and forces acting in the axial and normal directions at
         each nodal
    location
    """
```

```
# Get MachUpX wing input from argv
with open('IGE_case_one.json') as json_file:
    wing_dict = json.load(json_file)

# Adjusts input JSON file to contain user specified twist distribution for out
     of ground
# effect wing and the opposite twist distribution for the in ground effect
    wing
for i in range(10):
    wing_dict["wings"]["main_wing"]["twist"][i][1] = twist_distribution[i]
    wing_dict["wings"]["ground_effect_wing"]["twist"][i][1] = -
        twist_distribution[i]
with open('IGE_rewritten_wing_input.json', "w") as rewritten_wing_input:
    json.dump(wing_dict, rewritten_wing_input, indent = 2)

# Specifies input JSON for scene object, see Appendix A
input_file = "IGE_case_one_input.json"

# Initialize Scene object. This contains the airplane and all necessary
    atmospheric data.
my_scene = MX.Scene(input_file)

# Calculates the aerodynamic forces acting on the wing
my_forces = my_scene.solve_forces(dimensional=False, non_dimensional=True,
report_by_segment=True, verbose=False)

 ################################
 This portion of the code handles the cubic interpolation
 ################################
with open('IGE_rewritten_wing_input.json') as json_file:
    wing_dict = json.load(json_file)
```

```
initial_10_twist_loc = wing_dict["wings"]["main_wing"]["twist"]

locations = []
test_locations = []
x_coord = []
y_coord = []

for i in range(len(initial_10_twist_loc)):

  x = initial_10_twist_loc[i][0]
  y = initial_10_twist_loc[i][1]

  x_coord.append(x)
  y_coord.append(y)

# pass in 10 twist x and y valules to determine interpolating function
f = interp1d(x_coord, y_coord)
f_linear = interp1d(x_coord, y_coord, kind='linear')
f_cubic = interp1d(x_coord, y_coord, kind='cubic')

span_frac_array = distributions["traditional_airplane"]["main_wing_right"]["
    span_frac"]
twist_values_array = np.array(twist_values_array)
span_frac_array = np.array(span_frac_array)
interpolated_x_coord_list = []
interpolated_y_coord_list = []
replicated_inter_list = []

# This function interpolates twist value at every span fraction location
for i in range(len(span_frac_array)):
```

```
  interpolated_x = span_frac_array[i]
  #interpolated_y = f_linear(interpolated_x)
  interpolated_y = f_cubic(interpolated_x)

  interpolated_x_coord_list.append(interpolated_x)
  interpolated_y_coord_list.append(interpolated_y)

  replicated_inter_list.append([interpolated_x_coord_list,
      interpolated_y_coord_list])

# machupx requires that the twist initialization begins at a span fraction
# of 0.0 and ends at 1.0. This just inserts those values at the beginning
# end of the new interpolated twist array
new_interpolated_twist_list = []
for i in range(102):
    if i == 0:
        new_interpolated_twist_list.append([0, twist_distribution[0]])
    elif i == (len(span_frac_array)+1):
        #print("last twist node")
        new_interpolated_twist_list.append
        ([1.0, twist_distribution[-1]])
    else:
        new_interpolated_twist_list.append
        ([span_frac_array[i-1], interpolated_y_coord_list[i-1]])


new_interpolated_twist_list_reshaped = np.reshape(new_interpolated_twist_list,
     (102,2))
```

```
# I have to rewrite the json so that it contains the entire interpolated twist
    list
# so it doesn't overwrite it. I have validated that the values remain the same
    after
# calculating the forces and everything.
list_of_lists = list()
for row in new_interpolated_twist_list_reshaped:
   list_of_lists.append(row.tolist())

wing_dict["wings"]["main_wing"]["twist"] = list_of_lists

new_list_of_lists = []
for i in range(102):
  new_list_of_lists.append([list_of_lists[i][0], - list_of_lists[i][1] ])

wing_dict["wings"]["ground_effect_wing"]["twist"]= new_list_of_lists

with open('IGE_rewritten_wing_input.json', "w") as rewritten_wing_input:
   json.dump(wing_dict, rewritten_wing_input, indent = 2)


# the rewritten json file now contains a twist list that is 102 long, 2 longer
# than the number of nodes because I have to specify values at 0 and 1

input_file = "IGE_case_one_input.json"
my_scene = MX.Scene(input_file)
my_forces = my_scene.solve_forces(dimensional=False, non_dimensional=True,
report_by_segment=True, verbose=False)
twist_values_array = np.degrees(distributions["traditional_airplane"]
["main_wing_right"]["twist"])
```

```
span_frac_array = distributions["traditional_airplane"]["main_wing_right"]["
    span_frac"]
twist_values_array = np.array(twist_values_array)
span_frac_array = np.array(span_frac_array)

################################
 End of cubic interpolation portion
 ################################

# MachUpX calculates lift and drag for each semispan, adding them together is
    the
# total lift and induceddrag coefficient for the wing
CL_total_main = my_forces["traditional_airplane"]["inviscid"]["CL"]["
    main_wing_left"]
+ my_forces["traditional_airplane"]["inviscid"]["CL"]["main_wing_right"]

CD_total_main= my_forces["traditional_airplane"]["inviscid"]["CD"]["
    main_wing_left"]
+ my_forces["traditional_airplane"]["inviscid"]["CD"]["main_wing_right"]

# Extracts freestream velocity of scene for used for calculation of dynamic
    pressure.
# Specified in Appendix A
freestream_velocity = my_scene["traditional_airplane"]["state"]["velocity"]

# MachUpX defaults to run at sea level, the air density
#at sea level is 0.002378 slug/ft3
rho = 0.002378

################# DISTRIBUTIONS #################
"""
DEFINITIONS:
```

```
z_b: List of spanwise fractions from 0-0.5
twist: List of twist values applied at each section
right_section_CL: Section lift coefficient
right_section_CDi: Section induced drag coefficient
FZ: body-z force acting on each section
FX: body-x force acting on each section
section_area: section differential planform area
section_chord: section geometric chord
global_q: global dynamic pressure
right_section_CL_FZ: Section lift coefficient acting in the normal direction
right_section_CDi_FX: Section induced drag coefficient acting in the axial
    direction
"""

distributions = my_scene.distributions(verbose=False)
z_b = np.array(distributions["traditional_airplane"]["main_wing_right"]["
    span_frac"])*0.5
twist = np.degrees((distributions["traditional_airplane"]["main_wing_right"]["
    twist"]))
right_section_CL = distributions["traditional_airplane"]["main_wing_right"] ["
    section_CL"]
right_section_CDi = distributions["traditional_airplane"]["main_wing_right"]
    ["CD_i"]
FZ = distributions["traditional_airplane"]["main_wing_right"] ["Fz"]
FX = distributions["traditional_airplane"]["main_wing_right"] ["Fx"]
section_area = distributions["traditional_airplane"]["main_wing_right"] ["area
    "]
section_chord = distributions["traditional_airplane"]["main_wing_right"] ["
    chord"]
global_q = 0.5*rho*freestream_velocity**2
right_section_CL_FZ = []
right_section_CDi_FX = []
```

```
    for i in range(len(section_area)):
        right_section_CL_FZ.append(FZ[i]/global_q/section_area[i])
        right_section_CDi_FX.append(FX[i]/global_q/section_area[i])

    return CL_total_main, CD_total_main, z_b, twist, right_section_CL,
    right_section_CDi, right_section_CL_FZ, right_section_CDi_FX

if __name__=="__main__":

    # Select to have initial guess be a uniform twist distribution of 0 degrees.
    # Resulting JSON input file is given in Appendix B
    twist_dist = np.zeros(10)

    # Select to have initial guess be a uniform twist distribution of 8 degrees.
    # Resulting JSON input file is given in Appendix C
    #twist_dist = np.ones(10)*8

    # Select to have initial guess be a twist distribution calculated using Eq.
        1.29.
    # Resulting JSON input file is given in Appendix D
    #twist_dist = [6.706766629, 6.618571439, 6.356665636, 5.929007094,
        5.348590003,  4.633050042,
                  3.80412853, 2.887011828,  1.909566064,  0.901490431]

    # Total wingspan, used for calculation of of CL_hat and CD_hat
    b = 8.0

    # Root chord of rectangular wing, used for calculation of of CL_hat and CD_hat
    c_root = 1.0

    # Calls mydist function, passes in twist distribution specified above.
```

```
# Returns total CL and CD, list of span fraction locations (z_b), list of
    twist values
CL_total_main, CD_total_main, z_b, twist, right_section_CL,
right_section_CDi, right_section_CL_FZ, right_section_CDi_FX = mydist(
    twist_dist)

# Stores right_section_CL_FZ in list with naming conventions specified in this
     work
CL_tilde = []
for i in right_section_CL_FZ:
    CL_tilde.append(i*-1)

# Stores right_section_CDi_FX in list with naming conventions specified in
    this work
CDi_tilde = []
for i in right_section_CDi_FX:
    CD_tilde.append(i*-1)

# CL_tilde normalized by the chord length
CL_hat = []
for i in right_section_CL_FZ:
    CL_hat.append((i*-1) * (c_root/b))

# CDi_tilde normalized by the chord length
CDi_hat = []
for i in right_section_CDi_FX:
    CD_hat.append((i*-1) * (c_root/b))
```